7-20-2021

An Analysis of Capillary Flow in Finite Length Interior Corners

Samuel Shaw Mohler
Portland State University

Let us know how access to this document benefits you.

An Analysis of Capillary Flow In Finite Length Interior Corners

by

Samuel S. Mohler

A thesis submitted in partial fulfillment of the
requirements for the degree of

Master of Science
in
Mechanical Engineering

Thesis Committee:
Mark M. Weislogel, **Chair**
Raúl Bayoán Cal
Sung Yi

Portland State University
2021

Abstract

We analyze the mathematical robustness of slow massively parallel interior corner flows in low gravity environments. An interior corner provides a preferential orientation in low gravity environments. This is a luxury usually only found on earth. It also provides a passive pumping mechanism due to geometry of a conduit. The driving force for this flow is a pressure difference due to local surface curvature gradients. An alternative reasoning is that due to the geometrical constraints the interior corner surface energy is unbounded below. This results in the liquid wicking into corners indefinitely. Interior corner flow's main quantity of interest is the meniscus height $h(z,t)$. With this variable one can calculate an average velocity $\bar{w}$, flow rate Q, and volume of liquid in the corner V. Our study is different from most as it is highly in-depth look at finite domains, while the majority of previous solutions focus on similarity solutions of infinite, or semi-infinite domains. Boundary conditions, more specifically the functions that are assigned to the governing equation, play an integral role to meniscus height. We study a simplified problem of corners initially filled with quiescent liquid at $t = 0$, and boundary conditions are instantaneously applied when $t > 0$. Approximate asymptotic expressions are found for this process, but more importantly a method of approximating nonlinear heat equations as a sequence of linear heat equations is proved as a viable method for engineering purposes. Time varying boundary conditions are analyzed using a method of *model-approximation.*

This is where we simply remove the nonlinearity of the governing equation and insert a fitting term η. The method works surprising well for a range of constant and time varying boundary conditions. In all cases the relative error between solutions is less than 10%. This is a major theme of the thesis, that is, *force* initial value boundary value problems to be linear via a substitution and achieve results sufficient for engineering analysis. For parallel corners, volume can transfer between corners in a multiple corner system. This motivates formulating an ODE governing the average height $H(t)$ instead of meniscus height $h(z,t)$. We formulate an N corner start-up problem similar to the analysis of a single corner. This solution is only true for a quasi-steady process for creeping flows. In order to feed a corner fluid, manifold tubing is required. Tubing presents a drastic geometrical difference where manifold resistance is much greater then the corner. This means for parallel flows that the dynamics of the system is governed by the transients introduced by the corner's ability to store volume. Real world system fluid properties can vary from temperature, concentration, and other gradients. These effects alter the meniscus height. We consider temperature and concentration gradients which add additional terms to the spatial derivative side of the equation. The property variation is captured by only three axial location-dependent coefficient functions. Finally, corners that are pinned along the top edge are shown to have a governing equation with a similar form to meniscus height $h(z,t)$ equation. The simplifications used to establish analytical results can also be utilized for numerical solutions, difference being that the new quantity of interest is now the axially-dependent contact angle function $\theta(z,t)$, which is now free to pivot about the top edge of the groove.

Dedication

To mum for the voice

To dad for the mind

To bro for the arts

To friends for the break

To Mark for the chance

and to my wife Anaïs, my everything

for everything.

Contents

List of Figures

x

List of Tables

1 Introduction

This thesis is an analysis inspired by a proposed design for a CO_2 scrubbing system for space environments. A scrubbing system is any system that removes CO_2 from the air in a closed environment. The design is inspired by current submarines scrubbers that utilize gravity driven thin film flows. The gravity force is replaced with a combination of surface tension, wetting characteristics, and conduit geometry. Surface tension is a bulk behavior of surface molecules being attracted to each other. It can be measured and used as a parameter in equations. Wetting characteristics are encoded in the the contact angle of a liquid θ, which is defined as the angle a liquid makes when wetting a locally flat surface. In space environments the gravity force is negligible compared to surface tension. Negligible is defined as the Bond number being sufficiently small, or $\mathsf{Bo} = \rho g R^2 / \sigma \ll 1$. Surface tension allows for a passive driving force with no moving parts or pumps. Our design proposes to replace the gravity force with surface tension and utilize interior corner flow. Interior corner flow is flow along the sharp corners of containers because of dominate surface tension pressure gradients. Sharp is quantified by the Concus-Finn condition [1]. It sets a mathematical limit on the combination of fluid contact angle and the half-interior corner angle, $(\alpha + \theta) < \pi/2$. An effective thin film is built up from thousands of parallel interior corners of finite length. Currently there is no foundation of analysis for interior corner flow in finite domains. The current state of knowledge lay in semi-infinite or infinite domains [2, 3]. A recent

work analyzed this flow in a finite domain with the caveat of symmetric zero boundary conditions [4]. Our work greatly advances the transient modeling of interior corners in finite domains with *arbitrary* boundary conditions. Furthermore, the methods developed herein promise a novel method to estimate nonlinear diffusion equations in finite domains. Single corner analysis in chapters 1-4 are an in-depth development of the equations and solution for interior corners in finite domains. Chapters 5 we consider the additional effects of changing temperature and concentrations. These additional gradients create a larger system of governing equations, and scale analysis show first order effect are all axial $C(z,t), T(z,t)$. The time scales of the concentration and temperature equations are much less than the momentum, and this make the thermophysical steady-state with axial variations. The effects lead to a new governing equation for meniscus height $h(z,t)$. All the thermo-physical effects are encoded by three coefficient functions $a(z), b(z), c(z)$. Analysis of these functions produce estimates on liquid property variations. Chapter 6 suggests the immediate future work of considering fully filled open channel interior corners with a moving contact line. We make a change of perspective and notice that the contact angle $\theta(z,t)$ is the true independent quantity, and we formulate a new governing equation. This new equation is highly nonlinear, but in a final parting we present an incredible approximation method to estimate the dynamics of this scenario.
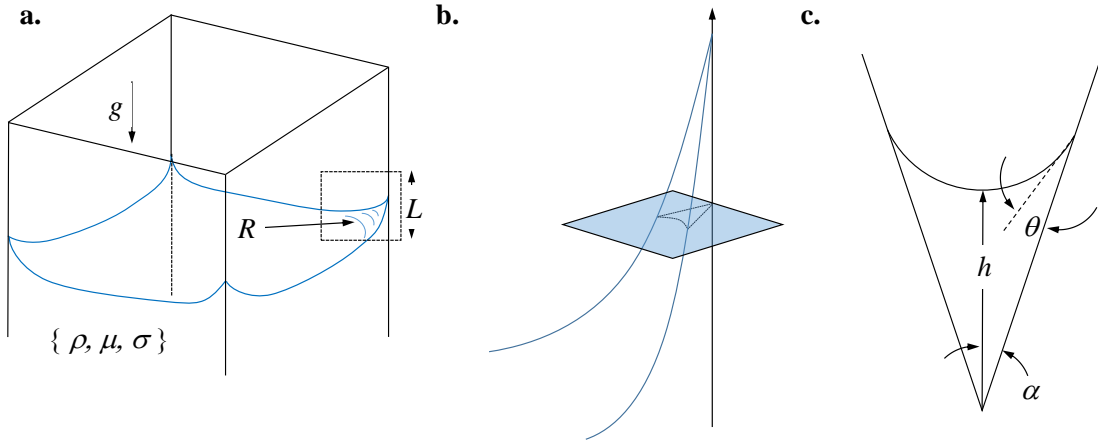
FIGURE 1.1: In gravity is **a.** and we see a slight rise in the wicking tip L. The effects of surface tension become important in the dash line area when R is small. For **b.** we've isolated the dashed lined area and highlighted a cross planar section. Interior corner flow models the behavior around this wicking tip and considers a cross-sectional mass balance. In **c.** we sketch this cross planar view of the wicking tip. The variables involved in (1.1),(1.2) and (1.3) are all present.

1.1   Key Assumptions

The scope of this research is to study the governing equations of interior corner flow and to interpret its solutions to aid in an engineering design. In the literature the phrase corner is sometimes replaced with *triangular-groove* [5] or *open-wedge* [6], but the governing equations are the same. All interior corner flow must satisfy three major conditions in order to arrive at the governing equation.

Negligible Gravity Force   These assumption are summarized in figure 1.1. The first is a requirement is on the Bond number,

$$\text{Bo} = \frac{\rho g R^2}{\sigma} \ll 1. \tag{1.1}$$

4

This is a ratio of the gravity force to surface tension force. On earth this condition can be met at very small length-scales. One can see with the naked eye interior corner effects looking at a container with sharp corners filled with liquid. Right around the interior corner the length scale is very small $R \to 0$, and surface forces become comparable to the gravity force. The gravity force fights to flatten all points with respect to the z-direction established by the earth's surface. The surface tension force fights to flatten the surface force with respect to outward normal established by the free-surface. Close to the corner these forces are in opposite direction. This balance of forces results in the tip of the liquid to be slightly higher than the bulk. We however are interested in low-g environments where $g \sim \mathcal{O}(10^{-6})$. With the gravity force negligible everywhere, equilibrium surfaces become much more exotic. The study of these equilibrium surfaces was the focus of early investigations and summarized greatly in [7, 8].

Length Scales The second assumption is on the meniscus height h to the flow direction length scale L. This height is the ray which bisects the interior corner and ends at the liquid surface. We follow [9] and call this the *center-line meniscus height*. Our analysis begins with the assumption that our wedges have finite length $L < \infty$. This introduces then a length scale condition that

$$\epsilon^2 = \left(\frac{h}{L}\right)^2 \ll 1. \tag{1.2}$$

This assumption greatly reduces the Navier-Stokes equations leaving only the axial momentum equation and continuity. After mass is conserved, the governing equation is a differential equation for the meniscus height *function* $h(z,t)$. This one-

dimensional model is quite robust because of the condition is on ϵ^2, not ϵ. This means as long as $h/L \sim 0.3$, (1.2) is satisfied.

Concus - Finn The third condition is called the Concus Finn condition [1].

$$\theta + \alpha < \frac{\pi}{2} \qquad (1.3)$$

This requirement is a statement about non-existence to the minimum surface equation for the interior corner. Concus and Finn refined the broad statement of *non-existence* to *unbounded-solution*. The potential energy of the surface has an unbounded well if this condition is met. Force is the gradient of potential which gives rise to the pressures to drive the flow. In drop tower experiments the force of gravity can be momentarily reduced. This reduction of gravity combined with (1.3) exhibits a flow where the liquid tip rapidly advances along the interior corner. The short time scale of the flow offers much more useful transport applications. This flow can be seen on earth at your kitchen sink. Arrange two microscope slides and have their tips meet to make a sharp wedge. Dip this wedge into a fluid reservoir and observe the wicking tip. This conversion of surface potential to kinetic energy only goes so far. Once the wicking corner reaches the tip of the container the boundary conditions of the problem change and the model breaks down. This "kitchen-sink" experiment has been extended and the time scale made universal [10]. This work concludes this wicking occurs for all values of Bo, large or small.

1.2 A Passive CO_2 Scrubbing System

The entirety of this analysis is focused on answering engineering questions about a CO_2 scrubber for space cabins. Today air is scrubbed aboard the I.S.S. using a porous media. The scrubbing occurs at the gas-solid interface between the air stream and the porous media. For more details on this system refer to [11]. On Earth, liquid-gas interfaces scrub the air on submarines, and they do it very efficiently [12]. This has motivated harnessing the fundamental physics used in the submarine. On the submarine, gravity is the driving force for a thin film flow. The thin film creates large surface area for the liquid-gas interface chemistry to occur. This chemistry involves the molecular interactions between the gas and liquid. The CO_2 taken up by the scrubbing liquid is then boiled off. Buoyancy forces drive the CO_2 gas bubbles out of the scrubbing liquid. The question is how do you attain a stable, large surface-area, thin-film flow in space.

Because we are interested in space, we only investigate situations where (1.1) holds. This means we do not have the luxury of using the gravity force to create a thin-film flow. We instead use parallel interior corners which give rise to a flow direction and a large surface area. A comparison of the two scenarios is given in figure 1.2. This simplified sketch is highly idealized. Thousands of corners are needed to create enough surface area. Considering the risks involved with space systems, thousands of corners require some amount of theoretical confidence. To complicate things even more, each corner has a restriction on its length L. Because of this, the design requires banks of massively parallel units arranged in series. The most current experiment is set to test a bank of 512 interior corners flowing in parallel. This massively parallel-series system mimics another terrestrial fluid transport device, the

7

$A_s \sim (f\bar{H}N)L$

Bo $\ll 1$

$\Delta P \sim \sigma(\dfrac{1}{H_2} - \dfrac{1}{H_1})$

$Q_1 \quad Q_2 \quad Q_3 \quad Q_k \quad Q_{N-1} \quad Q_N$

Bo $\gg 1$

$\Delta P \sim \rho g \sin(\theta)$

$A_s \sim WL$

Q_{out}
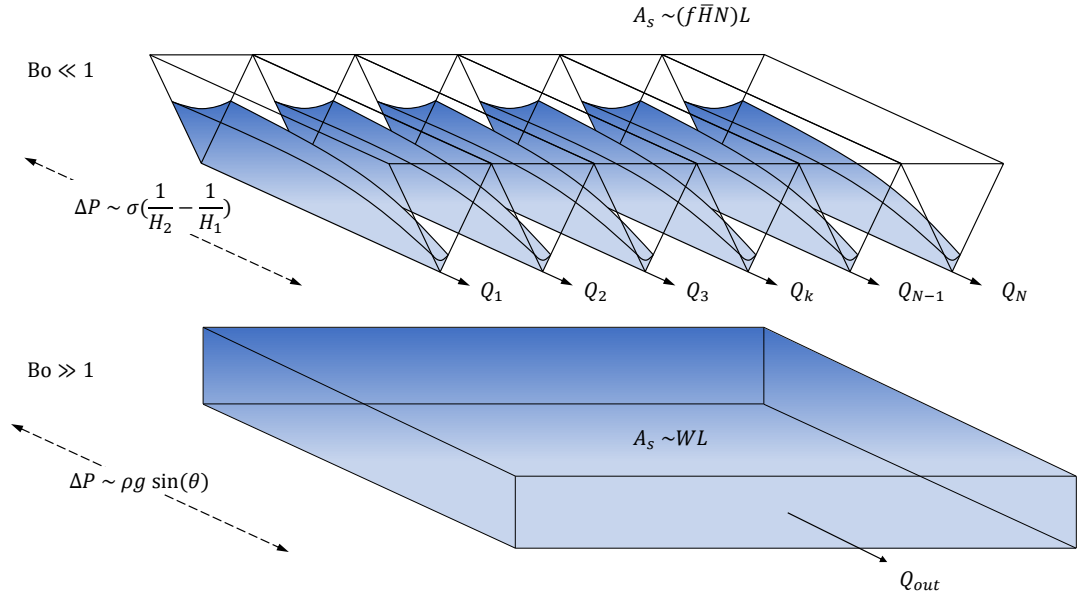
FIGURE 1.2:   An equivalent gravity driven thin-film can be simulated with several parallel corners.

tree. Enormous amounts of parallel flowing elements allows for a robust system. A tree maintains a steady state function even in harsh environmental conditions. It is understood that capillary action alone cannot account for getting liquid to the upper leaves. The trunk of a tree regardless has a flow rate Q thru it. We model that corner flow is occurring in air filled cavities of leaves and roots. This rationale for utilizing interior corner flow has been implemented, prototyped, and tested. Experiments have investigated steady-state operation, start-up transients, and extreme flow rate regimes have been preformed [13]. The largest number of corners tested to date has been 16 [14]. This number is orders of magnitudes below the necessary number of corners needed. Analytical predictions will help to build confidence for future experiments involving thousands of corners. If these massively parallel experiments agree to the theory, then the solutions can help guide designs. We follow a classical approach to

P_{atm}

P_{out}

N Generations

ΔP_{pump}

Q

$\Delta P_{\text{pump}} = QR_{\text{trunk}}$

CO_2 Rich Air

2^N Corners

$P_{\text{out}} - P_{\text{in}}$

N Generations

P_{grd}

P_{in}
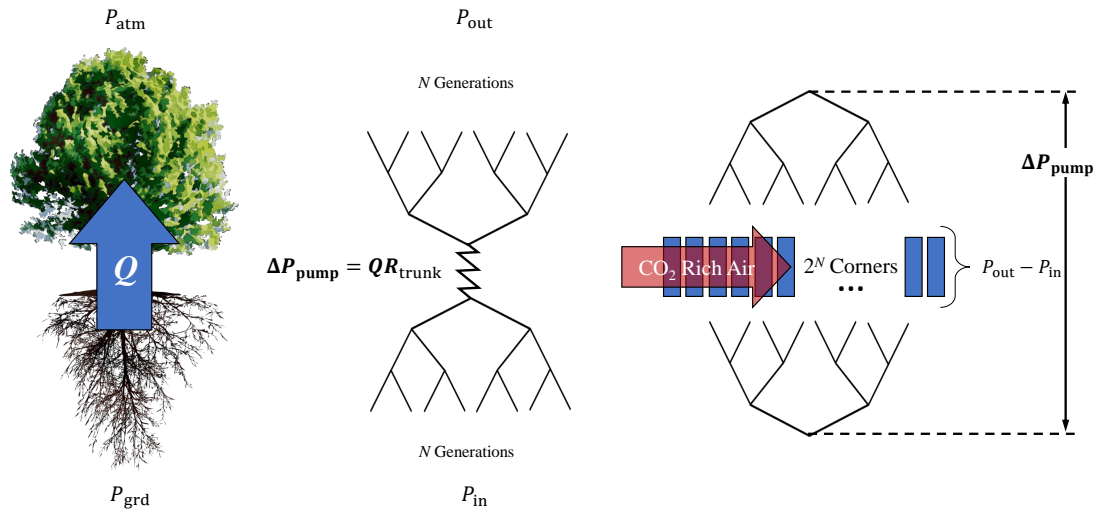
FIGURE 1.3: A schematic of the analogy of parallel interior corners to a tree pumping liquid. Leaves, trunk, and roots are modeled as circuit elements. Connecting the leaves to the roots creates a closed loop. A pump is required to resupply the liquid pumped by the interior corner.

study rigorously an individual finite corner in hope to extend the results to a circuit analogy. Direct numerical simulation for thousands of wedges is infeasible. This is not to say that highly accurate numerical simulations of this flow are not underway. There have been many advancement on this front in recent years [15, 16]. However, just as the Maxwell field equations are never directly solved for large electrical circuit networks, we see no reason the direct computation of the Navier-Stoke equations should be done for this model. Moreover, today analysis of parallel micro-fluidic systems has seen success with [17]. Finally, heat resistance networks have served as a rapid first step in design for hundreds of years. The same can be said for fluid pipe networks. All of these networks originally came from research into governing equations. The results have then gone on to be automated into software which help speed up cheap numerical testing of parallel systems.

1.3 Literature Review

Capillary fluidics in micro-gravity environments was first a study of fluid statics, specifically the free surface. Early works began from Russian mathematicians who calculated several equilibrium surfaces [7]. Concus and Finn did work in several equilibrium surfaces as well summarized in [18], but critically determined (1.3) in [1]. This gave analytical rigor to make an analysis of interior corner flows and consider dynamical problems and velocity field calculations. We note that capillary rise is a much older problem dating back to Washburn in [19] and had been applied for years. Bressler made an early investigation of these "capillary grooves" by considering the increase of heat transfer due to evaporation at the tip in [20]. The cross sectional velocity fields were calculated soon after using a Galerkin boundary method in [21].

In the next decade more grounded application analysis emerged. Lenormand experimented with 2D etched networks causing increased imbibition and wetting in [22]. Theorizing the mechanism was this flow he went on to make flow-rate regimes and calculations. Ransohoff determined a dimensionless flow resistance and further more found approximations utilizing hydraulic diameters amounted in large errors [23]. Stability started to become investigated with Langbein in [24]. It is important to note that all the results of all these investigations lay on the assumption that the domain was infinite and similarity solutions were possible. The flow schematic was always some form of Figure 1.4. The main quantity of interest in the case of Washburn, Bressler, and of "capillary rise" was $\mathcal{L}(t)$, but in later years more details and predictions of $h(z,t)$ were to come.

The 1990's saw a large boom in the analysis, experimental, and numerical investigations of $h(z,t)$. These works verified the analysis with experiments done aboard drop towers, parabolic flights, and numerical calculations. Dreyer has some of the first of these work in [25], where he identified three time domains of transition in drop tower experiments. His investigation tracked the *leading* meniscus tip $\mathcal{L}(t)$ and affirmed the governing equation as an accurate model for the flow. We should note that a leading meniscus tip corresponds a stretching domain of a similarity solution analysis method. Dong later looked at square tubes and developed the use of dimensionless flow resistance as a viable analysis tool in [6]. Importantly at this stage it was shown that the imbibition rate was proportional to $(\sigma/\mu)^{1/2}$. Remarkable advancement on the governing equations of this flow was done by Romero & Yost [5]. They identified the distinct different nature of the solution if the groove was partially or fully filled. Their similarity solution methods as well created a path way for much more general-

11

$$P_{in} \sim -\frac{\sigma}{H_1}$$

$$\mathcal{L}(t)$$

$$h(0, t) = H_1$$

$$h(z, t) \sim F(\eta = \frac{z^2}{t})$$

$$P_{out} \sim \lim_{H_2 \to 0} -\frac{\sigma}{H_2}$$

$$h(\mathcal{L}(t), t) \to 0$$

$$z \in [0, \infty)$$
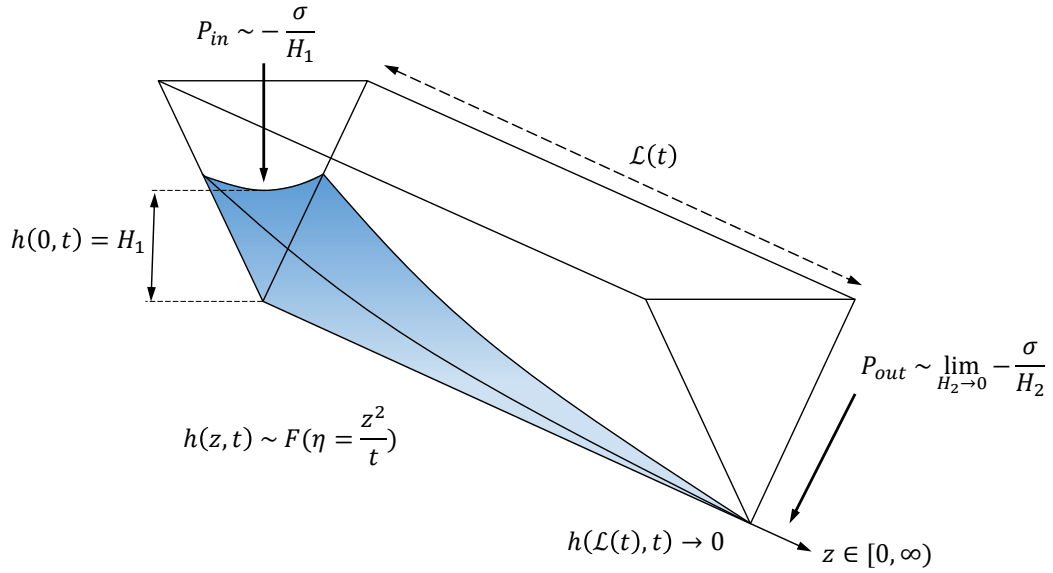
FIGURE 1.4: The semi-infinite domain problem or moving boundary problem require the end boundary to be zero. There are several different similarity solutions depending on the assigned boundary conditions. Solutions are possible for various assumptions imposed on $\mathcal{L}(t)$. However all these assumptions require $\mathcal{L} \to \infty$ and $t \to \infty$. Here we have assigned a constant height at $h(0, t) = H_1$.

ized solutions later on as well. Weislogel and Lichter essentially closed the book on interior corner flows with flat walls in [9, 26]. They generalized all similarity solutions and importantly connected specific power law values to different physical problems the solutions modeled.

There is one critical work by Peterson [27] in this decade we must discuss. Peterson was interested in capillary flow in wicking up grooves at an angle and enhancing heat transfer, similar to Bressler. The major quantity of interest was the "dry-out" location of the leading tip $\mathcal{L}(t) \to \mathcal{L}_0$. He had experimental data for this tip, and its location was proportional to the evaporation rates which could enhance heat transfer. Instead of a numerical investigation, Peterson *approximated* the nonlinear governing equation he derived for $\mathcal{L}(t)$ as a solvable Bernoulli type differential equation. Importantly an analytical solution was available for the later. His investigation was analytical and experimental, The predictions from this approximate model agreed with experimentation for a parameter sweep of Bond numbers Bo, Capillary numbers Ca, and various wedge geometry. In the coming chapters we do the same for the governing equation. Unlike Peterson, we compare numerical and analytical solutions for parameter sweeps.

After the 2000's the analysis of this interior corner flow shifted into perturbing initial and boundary conditions slightly. Weislogel investigated sinusoidal perturbed initial condition in an infinite column in [28], and considered compound capillary flow in the interior of a polygon in [29]. These bulk flow predictions motivated the use of this flow for prospective design solutions summarized in [30, 31]. This process of the analysis of the governing equation for this flow inspiring design is still active today referring to [14, 32, 33, 34]. The boundary condition of symmetric flat walls was relaxed

13

by Chen and Tang in [35, 36, 37, 38], he analyzed rounded and asymmetric corners and found asymptotic solutions. Su numerically studied variable shear stress distribution across the liquid interface in [39], This marks an early example of considering surface tension gradients long the wedge. Keep in mind this boundary condition variation violates the assumptions needed to arrive at the governing equation for $h(z, t)$, so numeric investigation was required. Su had no physical laws describing this shear stress distribution at the surface. It was only a assigned boundary condition. Deferentially wetted corner walls were analyzed analytically by Golliher in [40], this still followed the 1D model but instead modeled a changing contact angle due to surface wetting characteristics in manufactured corners.

In the most recent studies even more alterations to the boundary and initial conditions have been made, but even more applications of the analysis to different microgravity scenarios has been demonstrated. Dynamical boundary conditions with application to bubble migration in conduits was made by Weislogel in [3]. The draining of the bottom of cylindrical fuel tanks has been analyzed by McCraney [4, 15] Entire classes of corner wall geometry have been solved by Zhou in [41]. The governing equation in disguise was used to analyze parallel micro-fluidic channels for Lab-on-a-Chip applications by Calver in [17]. Everything discussed so far however all relied on similarity solution methods which were made possible due to a time varying domain $\mathcal{L}(t)$, infinite or semi-infinite domain $L \to \infty$, or symmetric zero boundary conditions $h(-L/2, t) = h(L/2, t) = 0$. The most far reaching analysis for this governing equation equation when it comes to finite domains was made recently by White in [42]. Here is was proven that the solution to the governing equation was stable in the Lyapunov sense. This will be a critical fact for us later on. The results requires

14

constant boundary conditions in finite domains which exactly what we address in Chapter 3. We are confident in our results and methods since in hind sight we are simply providing an explicit expression for a specific case of their work.

1.4 Mathematical Formulation

The formulation of this flow starts from the Naiver-Stokes equations with a lubrication approximation (1.2). Scaling for depended variables are motivated using Fig. 1.5 and Fig. 1.6. We will follow the derivation found in recent work by McCraney [4], for more details on scaling of the interface boundary conditions we refer back to the seminal work Weislogel & Lichter [9]. Our work is concerned with the solutions to the governing equations in finite domains not the derivation itself. We begin with the fundamental flow schematic found shown below in Fig. 1.5. The Navier-Stoke equations are made dimensionless using the scales found in Table 1.1. There are two geometrical function f, F_A which appear in both figures. These functions are determined by the geometry of Fig. 1.6. Importantly the general interface boundary condition may be solved to first order to conclude that the interface is a series of circular arcs along the z-axis. The constraint that this interface curve must be a circular arc make determining the expressions $f(\alpha, \theta), F_A(\alpha, \theta)$ and exercises in trigonometry. It is found by relating the cross-sectional radius of curvature R to the meniscus height h with $R = fh$ and is determined to be,

$$f(\alpha, \theta) = \frac{\sin \alpha}{\cos \theta - \sin \alpha}.$$

(1.4)

15

The area function $A_s = F_A h^2$ is determined to be,

$$F_A(\alpha, \theta) = f^2 \left(\frac{\cos \theta \sin \delta}{\sin \alpha} - \delta \right), \tag{1.5}$$

with $\delta = \pi/2 - (\alpha + \theta)$. In order to justify a one-dimensional model we compare the cross-sectional curvature the the aspect ratio

$$\epsilon^2 f \ll 1. \tag{1.6}$$

This condition can be stated in terms of the the perpendicular curvatures with some manipulation as

$$\frac{\epsilon}{L} \ll \frac{1}{hf} = \frac{1}{R}. \tag{1.7}$$

This comparison shows the dependence f has on the assumption as well as corner length. If the corner length becomes increasingly small (1.7) cannot be satisfied. However, this is just the same as failing assumption (1.2). This constraint is about curvature, angles, and liquid. This is because (1.7) is a comparison of approximate parallel curvature (left-hand side) to cross-sectional curvature (right-hand side). This condition is also a guide for corner design and liquid selection. The left hand side should be thought of as fixed by corner *length* scales. The right side constrains the *angle* in the model. The right hand side involves f, which is an expression that couples a fluid property θ and corner geometry α. Various values of f show how changing interior corner angle α or liquid can break this assumption. The main interpretation is to use narrow corners for a liquids. The most common half interior angle is $\alpha = 7.5°$.
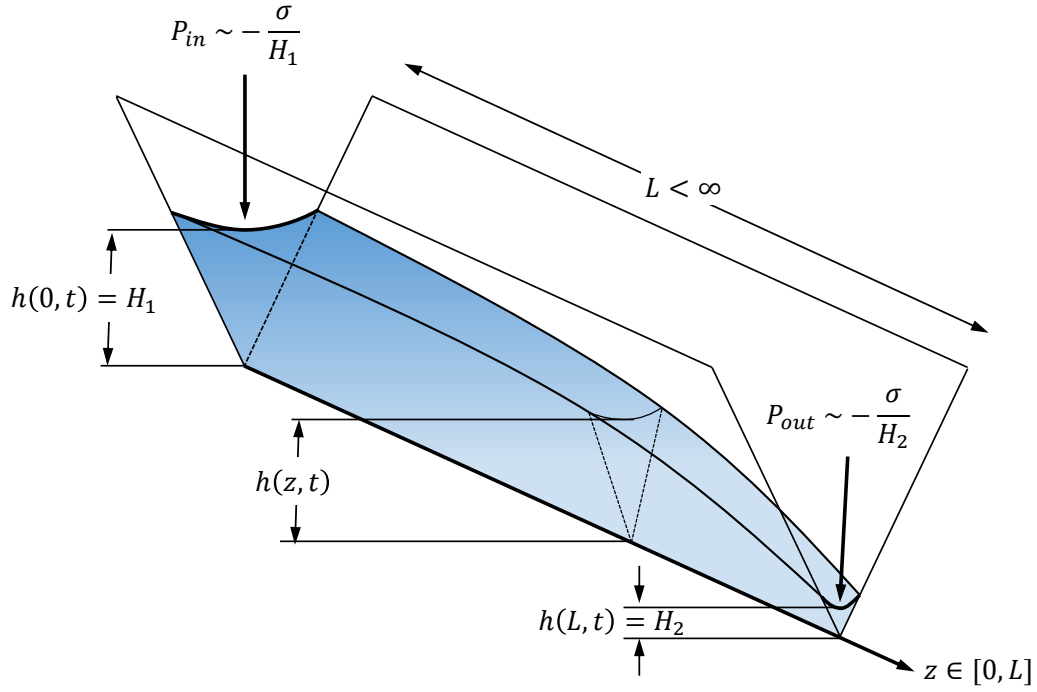
FIGURE 1.5: The governing flow schematic for interior corner flow in a constant finite domain $L < \infty$. The boundary conditions are constant with $h(0,t) = H_1$ and $h(L,t) = H_2$. When $H_1 > H_2$ flow is downstream as depicted here, if $H_1 < H_2$ flow is simply in the opposite direction.

TABLE 1.1: A summary of all dimensionless variables. The scaling is motivated by the geometry shown in Fig. 1.5, 1.6. Dimensional quantities are indicated with an uppercase prime. Here H is the dimensional height of the corner, and volumetric flow rate is denoted as Q.

Length	Velocity	Other
$x = x'/H$	$u = u'/\epsilon W_0$	$P = HfP'/\sigma$
$y = y'/H\tan\alpha$	$v = v'/\epsilon W_0 \tan\alpha$	$t = W_0 t'/L$
$z = z'/L$	$w = w'/W_0$	$A = A'/H^2 \tan\alpha$
$h = h'/H$	$W_0 = \epsilon\sigma\sin^2\alpha/\mu f$	$\epsilon = H/L$
	$\langle w \rangle = \langle w \rangle'/W_0$	$Q = Q'/W_0 H^2 \tan\alpha$

17
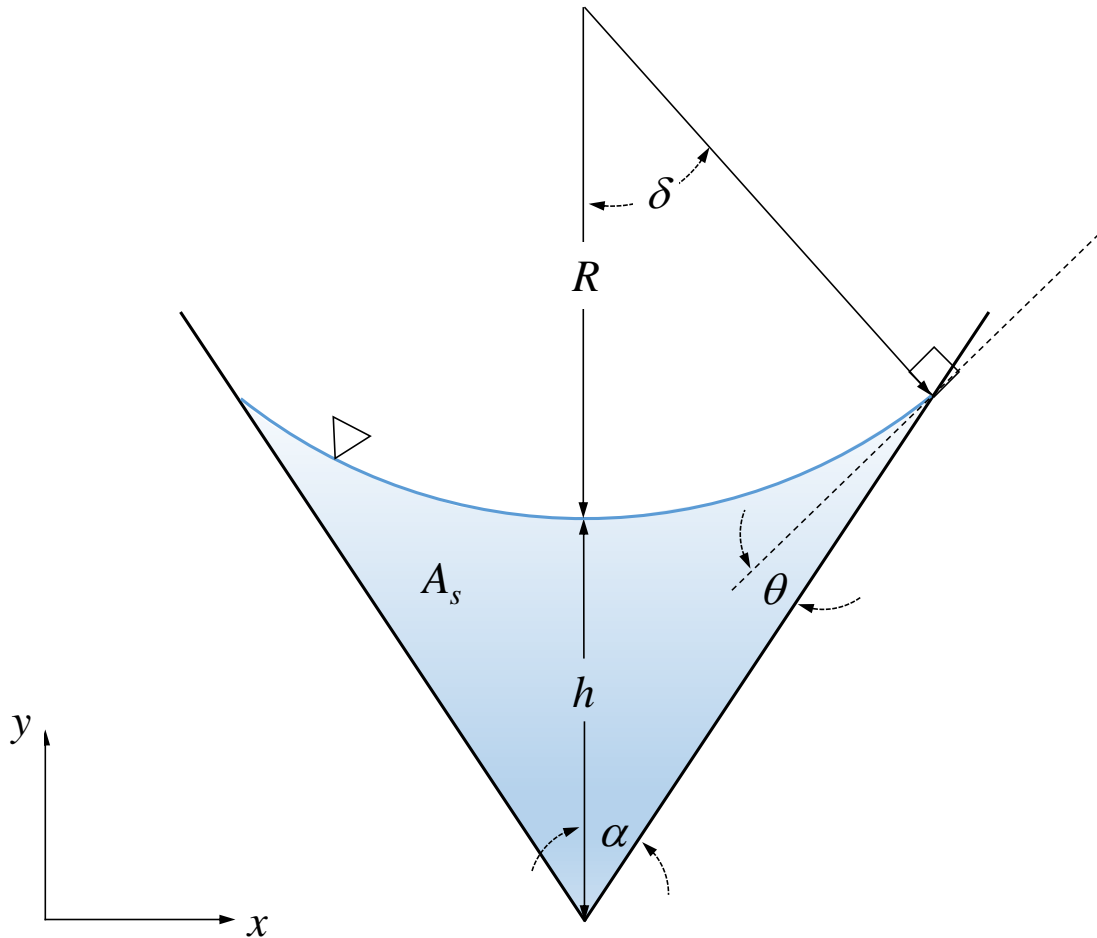
FIGURE 1.6: A geometrical cross sectional sketch of the interior corner. The tip of the corner should be set at the origin point $(0,0)$. It is an exercises in geometry to derive the relationship $A_s = F_A(\theta, \alpha)h^2$. There exists a function $f(\alpha, \theta)$ which relates the radius of curvature R to the meniscus height h. The free surface of the liquid is indicated by the triangle. We introduce the curvature angle $\delta = \pi/2 - (\theta + \alpha)$ here which will arise in later formulae.

With these assumption the full system of equations is determined to be

$$\epsilon^4 \mathsf{Su}^+ \frac{\mathrm{D}u}{\mathrm{D}t} = -\frac{\partial p}{\partial x} + \epsilon^2 \nabla^2 u, \tag{1.8}$$

$$\epsilon^4 \tan^2 \alpha \mathsf{Su}^+ \frac{\mathrm{D}v}{\mathrm{D}t} = -\frac{\partial p}{\partial y} + \epsilon^2 \tan^2 \alpha \nabla^2 v, \tag{1.9}$$

$$\epsilon^2 \mathsf{Su}^+ \frac{\mathrm{D}w}{\mathrm{D}t} = -\frac{\partial p}{\partial z} + \nabla^2 w, \tag{1.10}$$

$$\frac{\partial A}{\partial t} + \frac{\partial Q}{\partial z} = 0, \tag{1.11}$$

where $\mathsf{Su} = \sigma \rho H / \mu^2$, superscript $^+$ is geometrical scaling by $\sin^4 \alpha / f$, and $\mathrm{D}/\mathrm{D}t$ is the standard material derivative of fluid mechanics. The Suratman number can be thought of as a Reynolds number using a capillary velocity scale $V \sim \sigma / \mu$. One should appreciated the power of $\sin^4 \alpha$ in the inertial terms as well. This invokes even more that thin corners are viscous flow, this is reasonable as the thinner a corner becomes most of the flow is restricted to no-slip at the walls. All that can move is then just a thin strip of liquid interface at the "top" driven by surface pressure gradients. We have defined a non-dimensional Laplacian operator as well to be

$$\nabla^2 \equiv \sin^2 \alpha \frac{\partial^2}{\partial x^2} + \cos^2 \alpha \frac{\partial^2}{\partial y^2} + \epsilon^2 \sin^2 \alpha \frac{\partial^2}{\partial z^2}. \tag{1.12}$$

A solution comes from considering asymptotic solutions in powers of ϵ^2. In the limit of $\epsilon^2 \to 0$ and $\mathsf{Su}^+ \sim \epsilon^2$ the leading order effect leave only eq. (1.10). The governing equation for the velocity field in the axial direction is then,

$$\frac{\partial p}{\partial z} = \nabla^2 w, \tag{1.13}$$

19

with boundary conditions $w(wall) = 0, \nabla w(surface) = 0$. A very important property of eq. (1.13) is that it is proven that a solution exists and is unique for *any* function $\partial p / \partial z$. Understand the power of this statement. This means we may not know what the pressure gradient is but is valid to define an average flow-rate thru a cross sectional plane. We define an average velocity in thru the cross sectional plane by

$$\langle w \rangle = \frac{1}{A(z,t)} \int_{A(z,t)} w(x,y) \mathrm{d}A. \tag{1.14}$$

The problem closes when considering the pressure gradient scale relationship

$$\frac{\partial p}{\partial z} \sim \frac{\partial}{\partial z} \frac{1}{h},$$
$$\sim -\frac{1}{h^2} \frac{\partial h}{\partial z}.$$

Combining this with (1.14) we know in a $\langle w \rangle \sim -\partial h / \partial z$. Equality is achieved via an unknown proportionality term F_i such that

$$\langle w \rangle = -F_i \frac{\partial h}{\partial z}. \tag{1.15}$$

Early investigations [9] have proven numerically that $1/8 \lesssim F_i \lesssim 1/6$. The governing equation for $h(z,t)$ is determined by substitution of $A = F_A h^2$, (1.15) into (1.11) and is found to be

$$\frac{\partial h^2}{\partial t} = \frac{F_i}{3} \frac{\partial^2 h^3}{\partial z^2},$$

and re-scaling time to be $\tau = 3t/F_i$ we arrive at a very succinct governing equation

$$\frac{\partial h^2}{\partial \tau} = \frac{\partial^2 h^3}{\partial z^2}. \tag{1.16}$$

20

Already a world of analysis is available to us. This equation shows that the dynamics of $h(z, \tau)$ follow exactly the theory of nonlinear diffusion models where entire classes of solutions have been found in the past [43]. This is also why this work could have major implications in other fields, since *any* nonlinear diffusion model of the form (1.16) could use the results. In fact, we ourselves utilize analysis of nonlinear diffusion equations to claim solution existence and uniqueness to our model problem. We will drop the notation τ at this stage, since it is just a re-scaling by a constant value. This means herein all expressions with t are actually τ.

1.4.1 Initial Conditions & Boundary Conditions

For all of the analysis in chapters 1-4 we study eq. (1.16). This equation governs the dynamics of Fig. 1.5. Our last discussion is on the boundary and initial conditions assigned to this partial differential equation. The boundary conditions are applied at the inlet and outlet and shown in Fig. 1.5. There are three types of boundary conditions one could assign to this equation for $t > 0$ and $z = \{0, 1\}$ (Dirichlet, Neumann, and Robin). We will only consider Dirichlet boundary conditions where the value of $h(z, t)$ is prescribed at the inlet $z = 0$ and outlet $z = 1$. These are are called Dirichlet and in their most general form the prescribed values could be functions of time,

$$h(0, t) = H_1(t) \tag{1.17}$$

$$h(L, t) = H_2(t). \tag{1.18}$$

Next, our initial condition the meniscus height take for $t = 0$ and $z \in [0, 1]$,

$$h(z, 0) = H_0(z). \tag{1.19}$$

We have *compatibility* conditions we must require between $H_0(z), H_1(t), H_2(t)$ that is

$$H_0(0) = H_1(0) \qquad\qquad H_0(1) = H_2(0) \tag{1.20}$$

These are sufficient conditions for us so that we may claim that a solution to eq. (1.16) exists and is unique. It cannot be stressed how important this proof if to us. What it means is if we can *construct* some infinite series solution that is converging, we can be confident that it is converging to *the* solution. There are additional requirements on our initial and boundary function which all relate to solutions being physical.

$$0 < H_0(z), H_1(t), H_2(t) \quad \forall t > 0 \, \& \, z \in [0, 1] \tag{1.21}$$

$$\left| \frac{dH_0}{dz} \right| < \infty \quad \forall z \in (0, 1) \tag{1.22}$$

There is a much richer question of how relaxed the assumptions can be so that (1.16) admits a solution. We cite the work for Zischka & Chow [44] or other analysis of partial differential equations for more details on this topic. We have now fully set-up the general framework to investigate the dynamics of interior corner flows in finite domains. So let's begin.

2 Steady State Analysis

We first investigate the steady state solution for the meniscus height along the corner. This solution will help determine a steady state flow resistance function. For a single flow element, we will assume that the volume is constant. Our solution is presented in a generalized fashion valid for all boundary heights and initial conditions. The meniscus height is dependent on an average initial fill level $\mathcal{H}$ and the ratio of the boundary heights $\beta = H_2/H_1$. This non-dimensional parameter β is a measure of flow rate Q. Flow rate is maximum at $\beta = 0$, and minimum at $\beta = 1$. Invoking volume conservation, an expression for flow rate $Q(\beta)$ will be shown. For our CO_2 scrubbing application, the required flow rate is low such that $\beta \to 1$. This situation allows a Taylor expansion about $\beta = 1$ such that we can express boundary conditions as an infinite sum $\sum p_k(1 - \beta)^n$. Using this expansion, an asymptotic time evolution solution is found in chapter 3. Finally, we calculate the number of corners needed for a required flow rate given our maximum flow rate in a corner.

2.1 Generalized Steady State Solution

It has been shown many times over a steady state solutions exist for a single interior corner. This steady state solution has been utilized countless time for quasi-steady investigations in [3], and most of the work reference in Sec. 1.3. It is worth mentioning just how accurate this steady state solution is. Flight experiments have been
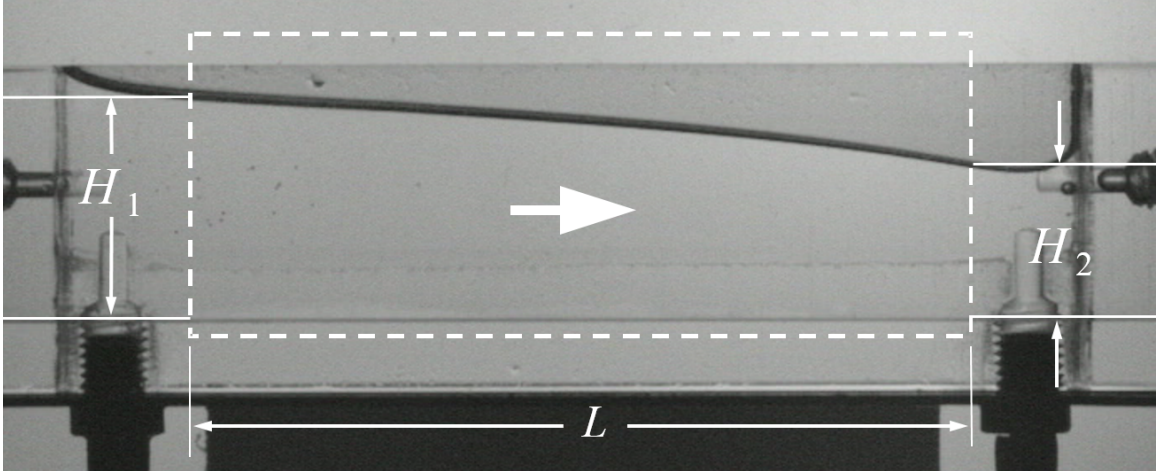
FIGURE 2.1: A low gravity aircraft experiment exhibiting a steady state profile. The test device is identical to 1.5. At the entrance and exit (1.6) fails to hold and the one-dimensional cross flow model breaks down. Our model is only valid for the region drawn in dashed white which covers most of the corner.

preformed in controlled low gravity environments and the solution we present has indeed been experimentally verified. Figure 2.1 is an image from these experiments and depicts illustration of this. In the immediate vicinity of the entrance and exit of the corner, stream-wise curvature cannot be neglected and the one dimensional cross-flow curvature model breaks down. Since we are following the formulation made in Sec. 1.4, unless stated otherwise, all equations herein are dimensionless via Table 1.1.

Our first problem to address is the steady state profile for constant boundary heights $h(0,t) = H_1$ and $h(1,t) = H_2$. The system of equations to solve is found by setting the governing equations time derivative to zero. Volume conservation in the corner takes an integral form. We leave the initial condition as a generic function $f(z)$ which satisfies eq. (1.20). This orients our analysis still within the framework described in Sec. 1.4. This generic function $f(z)$ should not to be confused with the geometric scaling function $f(\alpha, \theta)$ defined by eq. (6.1). This distinction should

be clear as $f(\alpha, \theta)$ has relevant two angular arguments. The steady state system of equations is then

$$0 = \frac{\partial^2 h^3}{\partial z^2} \tag{2.1}$$

$$H_1/H = h(0)$$

$$H_2/H = h(1)$$

$$f(z) = h(z, 0)$$

$$0 = \frac{d}{dt} \int F_A h^2 dz. \tag{2.2}$$

The steady state solution is found from integrating (2.1) twice and applying the boundary conditions to find

$$h(z) = (H_1^3 + (H_2^3 - H_1^3)z)^{1/3}. \tag{2.3}$$

By defining a non-dimensional parameter $\beta = H_2/H_1$, this ratio is independent of scale as well. Using β, we express the steady state solution as

$$h(z; \beta) = \frac{H_1}{H}(1 - (1 - \beta^3)z)^{1/3}. \tag{2.4}$$

We would like our solution to be expressed in tunable parameters such as a fill level and flow rate. This is the overall goal for all analysis, to define solutions (the unknown) in terms of initial and boundary conditions (the known). To achieve this we must express the steady state independent of H_1 and express the boundary height ratio as a function of flow rate $\beta(Q)$. We determine H_1 using our volume conservation integral (2.2). Since it is a conserved quantity we equate the initial volume in the corner at

25

$t = 0$ to the steady state volume when $t \to \infty$.

$$\int_0^1 F_A f^2 \, \mathrm{d}z = \int_0^1 F_A h^2 \, \mathrm{d}z \tag{2.5}$$

For the de-pinned case the area function F_A is a constant and may be factored out. This factoring is precisely why things get complicated in chapter 7. It is here we must make some assumption on the initial condition $f(z)$. The simplest sub problem is the *start-up problem* where at $t = 0$ the corner is at a constant fill level H_0. This corresponds to a dimensional relation,

$$H f(z) = \begin{cases} H_1 & z = 0 \\ H_0 & 0 < z < 1 \\ H_2 & z = 1 \end{cases} \tag{2.6}$$

This constant initial condition is sufficient for any $f(z)$. That is even for a complex initial condition $f(z)$ with lots of variation we could idealize a start up problem. This is because we can always find an equivalent H_0 for any initial condition $f(z)$. All we must do it take the root mean square of the arbitrary function $f(z)$.

$$H_0 = \left(\int_0^1 f(z)^2 \right)^{1/2} \tag{2.7}$$

We substitute (2.6) and (2.4) into (2.5) and preform integration. This yields our expression for H_1 as

$$H_1 = H_0 \sqrt{\frac{5(1 - \beta^3)}{3(1 - \beta^5)}}. \tag{2.8}$$

Now we substitute (2.8) into (2.4) to obtain our general steady state solution. We

26

plot this function in figure 2.2 and glean physical implications of values of β.

$$h_s(z) = \frac{H_0}{H}\sqrt{\frac{5(1-\beta^3)}{3(1-\beta^5)}}(1-(1-\beta^3)z)^{1/3}. \tag{2.9}$$

For $\beta > 1$, we have flow reversal. This makes sense as flow direction is always in the direction of the smaller boundary heights. Because of this, we will restrict ourselves to only studying $\beta \in [0,1]$, and will always keep the convention that $H_2 < H_1$. The most troublesome case is when $\beta = 0$. This can occur in two separate ways. The first is if $H_2 = 0$, which unfortunately corresponds to an infinite pressure for $P \sim -1/H$. The second is if $H_1 \to \infty$, which is infinitely wrong. We can side step these headaches by relying on the physical nature of a corner's design. In order to deliver fluid to the corner manifold tubing must be introduced. If the right pressure increases to much the meniscus height will drop down below the exit outlet and bubble ingestion will occur. This puts a lower limit for the value H_2 avoiding any infinite pressure.

Another point to add is the scaling made in table 1.1. We now have 4 scales of height to choose from namely the height of the corner H and H_0, H_1, H_2. If we rescaled all terms by the initial fill level H_0 instead of H all expressions look much simpler. This is why we suggest a scaling by H_0 not H, as is done in previous works We will carry the same scaling formulation as previous work accept for this one scale.

Using (2.9) we can calculate a dimensional flow rate thru the corner as $Q = A\langle w \rangle$. With some algebraic manipulation we can express flow rate purely in terms of liquid and corner parameters and H_0 and β.

$$Q'(\beta) = -\frac{H_0^3 F_A F_i \sigma \sin^2 \alpha}{3\mu f L}\sqrt{\frac{5^3(1-\beta^3)^5}{3^5(1-\beta^5)^3}} \tag{2.10}$$
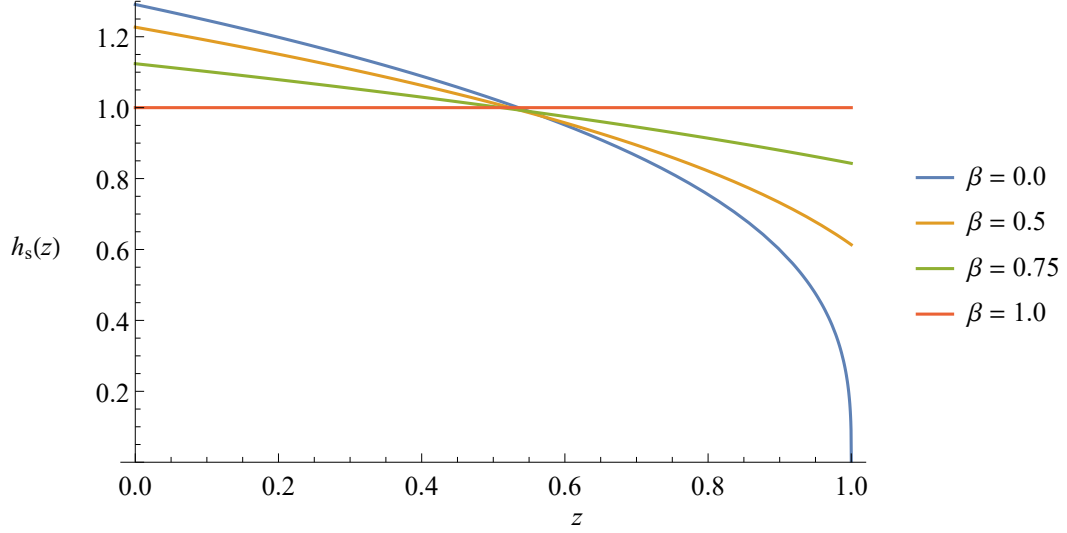
FIGURE 2.2: The side profile of an interior corner. h is the centerline meniscus height. Is in the direction left to right. Various values of β are plotted with an initial fill level of $H_0 = 1$. When $\beta = 1$ the boundary heights are equal and there is no flow rate. When $\beta = 0$ the flow rate is at a theoretical maximum.

It has been shown that suitable approximations for F_A and F_i are $\tan(\alpha)$ and $1/7$ respectively. Using these approximations, the scale flow rate is

$$Q' \sim \frac{\sigma(H_0 \sin(\alpha))^3}{21\mu f L \cos(\alpha)}. \tag{2.11}$$

If the geometric corner properties are constant, this scale is highly sensitive to our initial fill level H_0. Flowrate naturally is quite sensitive to corner geometry α as well, which is expected. As corner get wider there is more available interface area to transport liquid.

The non-dimensional form of (2.10), which is found using (2.11), is

$$Q(\beta) = -\sqrt{\frac{5^3(1-\beta^3)^5}{3^5(1-\beta^5)^3}}. \tag{2.12}$$

28

Now (2.12) tells us an analytical form of $\beta(Q)$ is impossible. This is because it would require inverting a fifth order polynomial. This forces us to either graphical inversion or approximate methods. In the next section we will develop asymptotic series based on β. This will be critical in developing the transient solution.

2.2 An Asymptotic Expansion Parameter ϕ

We can now utilize (2.9) to express the steady state as an asymptotic series. From figure 2.2 we see that for $\beta \sim 1$ model slow creeping flows. Recall the driving force is a difference in local curvature which is proportional to meniscus height. So if the inlet and outlet meniscus heights are almost the same $\beta \approx 1$, then there is not much of a pressure gradient to drive any flow. This can also be seen from (2.12). Because of this, in all of our taylor expansions we will choose to expand about $\beta_0 = 1$. We will expand (2.12) about $\beta = 1$ up to $\mathcal{O}((1 - \beta)^3)$ as an example. We also define a new parameter $\phi = 1 - \beta$. This new parameter is simply a convenience to make the equations simpler. This expansion can be done in software such as `Mathematica` or `Maple`. The first three terms are given as an example

$$h(z) = 1 + (z - \frac{1}{2})\phi + (-z^2 + \frac{1}{2}z + \frac{1}{24})\phi^2 + \mathcal{O}(\phi^3) \tag{2.13}$$

The general form of this expansion is a series in powers of ϕ with increasing coefficient polynomials $p_k(z)$ of order k.

$$h(z) = \sum_{k=0}^{\infty} p_k(z)\phi^k \tag{2.14}$$

29

If we evaluate the coefficient polynomials $p_k(z)$ at the boundary we form an infinite series. This series converges since we've ensured $\phi < 1$, $k \geq 0$, and $z \in [0,1]$ The polynomial evaluated at a specific z gives scalar numbers $p_k(0)$ and $p_k(1)$. These numbers again can be calculated using software such as Mathematica. As an example here are the first three terms of the boundary value series. Figure 2.3 plots the first 15 values of these coefficients.

$$h(0,t) = 1 + \frac{1}{2}\phi + \frac{1}{24}\phi^2$$
$$h(1,t) = 1 - \frac{1}{2}\phi - \frac{11}{24}\phi^2$$

We will from now on refer to the constant coefficients $p_k(0)$ and $p_k(1)$ as $\{A_k, B_k\}$ respectively. This allow us to form our boundary value series

$$h(0,t) = \sum_{k=0}^{\infty} A_k \phi^k \tag{2.15}$$

$$h(1,t) = \sum_{k=0}^{\infty} B_k \phi^k, \tag{2.16}$$

and we are now ready to look for an asymptotic transient solution of the form

$$h(z,t) = \sum_{k=0}^{\infty} h_k(z,t) \phi^k \tag{2.17}$$

There is one more expansion that is of interest. That is expanding (2.12) about $\beta_0 = 1$. Since we are setting out to determine an asymptotic solution for $h(z,t)$ with respect to the parameter ϕ, It would be helpful to have a quick calculation to see if a given flow rate justifies a linear approximation. A two term taylor series of (2.12)
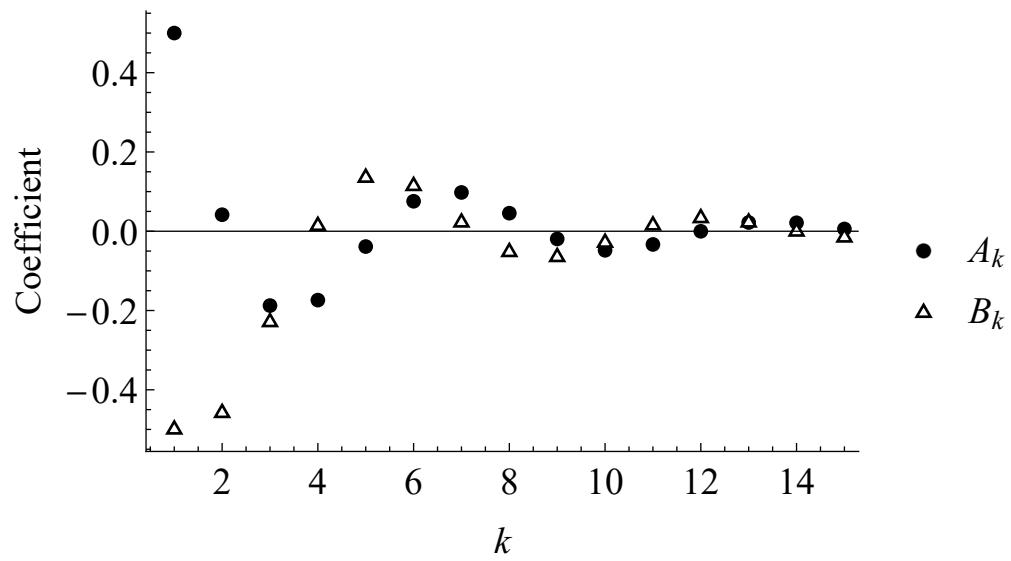
FIGURE 2.3: The boundary value series are plotted for $k \leq 15$. This sequence of numbers is conditionally convergent as well. For $k > 15$ the coefficients become quite negligible, however we will need several terms later on to model the nonlinear effects.

gives

$$Q = \phi - \frac{1}{2}\phi^2 + \mathcal{O}(\phi^3). \tag{2.18}$$

This approximation can be inverted analytically which yields

$$\phi = 1 - \sqrt{1 - 2Q}. \tag{2.19}$$

From (2.19) we can see that if $Q \ll 1$ then our asymptotic expansion parameter is indeed small. Figure 2.4 is a plot comparing the exact and approximate flow rate inversion. as well as the relative error of the approximation. We have marked where %10 error occurs as well. Remarkably this inversion is sufficient for over half the domain of Q, which is limited by ingestion at $\beta = 0$. However, we could select several expansion of (2.12), for instance, if we expand about $\beta_0 = 0$ we get insight to variations around nearly maximum flow rates. However, looking at figure 2.4 we see that (2.18) does quite a good job of an inversion for small $Q < 0.5$.

2.3 A System Pump Curve for The Corner

The steady state analysis so far can help give an analytical system pump curve for the interior corner. This curve can help characterize the ability to pump liquid in low gravity designs. To develop a pump curve we want to express $\Delta P(Q)$. One thing should be evident just from this definition alone. Since we already know there is a *maximum* flow rate $Q \approx 0.717$ corresponding to $\beta = 0 \therefore H_2 = 0$, and given that have shown $P = -1/fH$, we must expect this curve to diverge to infinity quite rapidly. This is exactly why we need several thousand corners in parallel to achieve a large flowrate.

32
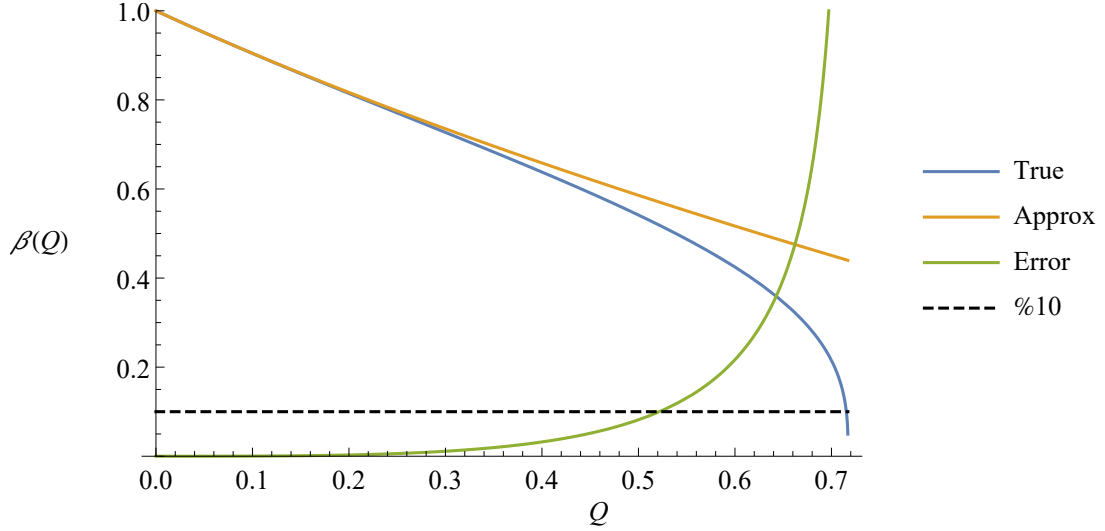
FIGURE 2.4: The approximate inversion (2.18) is compared to the true graphically inverted (2.12). The domain of allowed values is $Q \in [0, (5^3/3^5)^{1/2} \approx 0.717)$. The relative error between the curve diverges as $Q \to 0.717$ which is expected. What is surprising however is the approximation is under %10 (black dashed line) for nearly %70 of the domain

The pressure gradient across the corner can be expressed in terms of the boundary heights H_1 and H_2. From scaling the Navier-Stoke equations with the aspect ratio $\epsilon = H/L$, we know this pressure is valid up to $\mathcal{O}(\epsilon^2)$. The non dimensional pressure gradient is

$$\Delta P = \left(\frac{1}{H_2} - \frac{1}{H_1} \right). \tag{2.20}$$

Multiply the left hand side by $1 = H_1/H_1$ and utilizing (2.8) we derive,

$$= \left(\frac{1}{H_2} - \frac{1}{H_1} \right) \frac{H_1}{H_1},$$

$$= \frac{1}{H_1} \left(\frac{1}{\beta} - 1 \right),$$

$$\Delta P = \left(\sqrt{\frac{3(1-\beta^5)}{5(1-\beta^3)}} \right) \left(\frac{1}{\beta} - 1 \right).$$

33
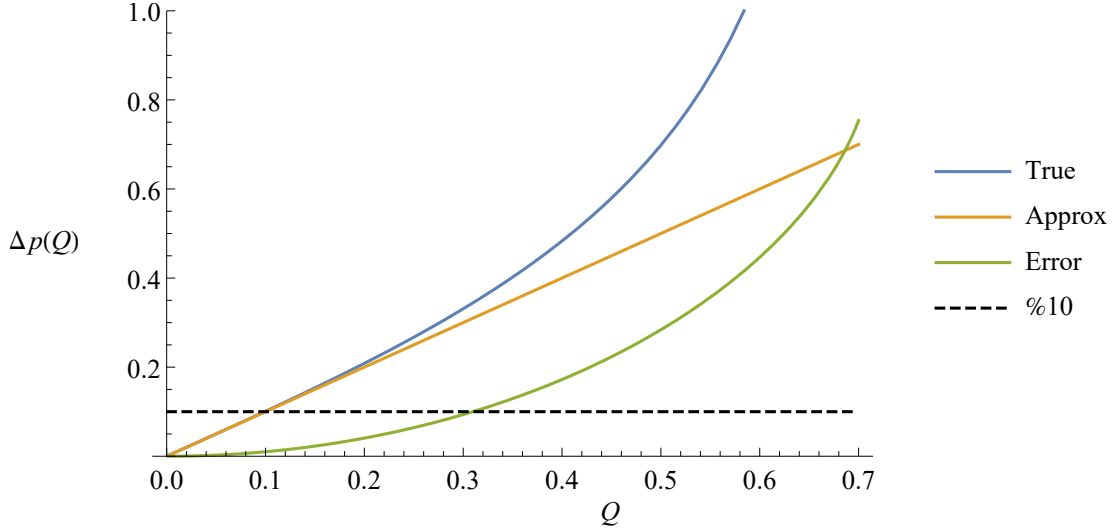
FIGURE 2.5: The relative system pump equation is plotted in the same manner as Fig 2.4. We have indicated a %10 error at the dashed black line. A first order approximation for ΔP, we can see is not as good as it is for $\beta(Q)$. However identifying an upper bound for linearization is still a useful result

In order to plot a system curve we must use a composition with $\beta(Q)$. However using (2.18) we can also preform *another* expansion about $Q = 0$. This will allow us an analytical system pump curve expression. But more importantly it allows us to see exactly when a corner behaves like a circuit with linear resistance. Expanding $\Delta P(\beta(Q))$ about $Q = 0$ we find that,

$$\Delta P(Q) \approx Q + \mathcal{O}(Q^3) \tag{2.21}$$

Which means circuit have linear flow resistance up to $\mathcal{O}(Q^3)$. We can compare this in figure 2.5 conclude that as long as the non-dimensional flow rate in a corner satisfies $Q \lesssim 0.3$, the system component can be linearized.

2.3.1 Number of Corners

The largest concern for these corners is the problem of bubble ingestion. If the flow rate becomes too high in one of the corners the leading edges H_2 will dip below an exit hole at the bottom of the corner. This gap will form bubbles because the once an opening occurs the negative pressure draws air into the line. The negative pressure as well draws the fluid towards the hole but the mass of the fluid causes it to move slower. The imbalance causes more air to be drawn in before the the whole is closed forming a bubble. This process would continue to persist as well if the pressure gradient is maintained across the inlet and outlet of the corner. In more extreme cases dry out can occur in a corner making a corner become effectively useless. We would like to avoid this ever happening. A first estimate is then how many corners would system need to ensure we likely avoid bubbles. Figure 2.6 is a diagram of an idealized parallel circuit of corners. The question is how many corners would be needed to avoid ingestion. For this section we will use dimensional expressions. By conservation of mass we know the flow rate thru the corners must sum to the required Q. So for N corners we must have,

$$Q_{req} = \sum_{n=1}^{N} q_n.$$
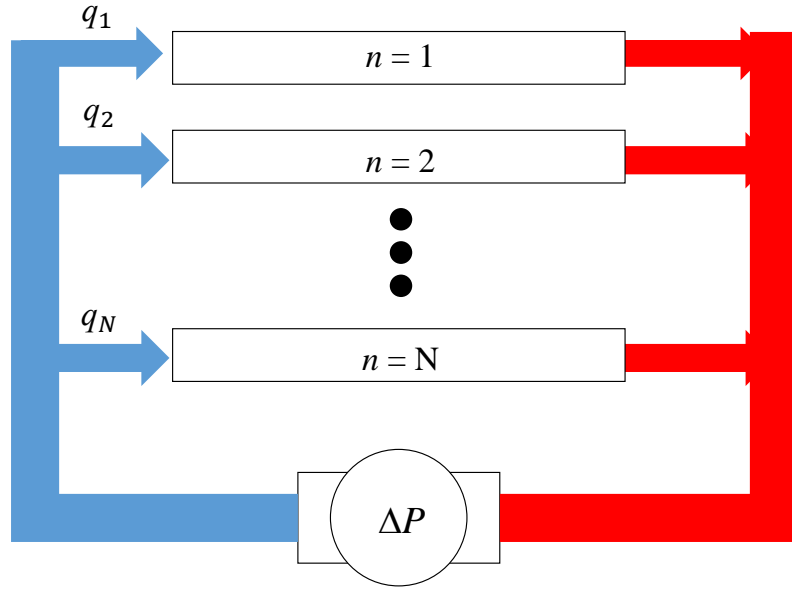
FIGURE 2.6: A system diagram of parallel corners acting as a flow separator. Each corner is counted by the index n.

Using (2.10) we come up with a maximum flow rate thru each corner $\beta = 0$. We have to idealize that the initial fill level in every corner is H_0.

$$
\begin{aligned}
&= \sum_{n=1}^{N} \frac{H_0^3 F_A F_i \sigma \sin^2 \alpha}{3 \mu f L} \sqrt{\frac{5^3 (1 - \beta^3)^5}{3^5 (1 - \beta^5)^3}} \\
&\leq \sum_{n=1}^{N} \frac{H_0^3 F_A F_i \sigma \sin^2 \alpha}{3 \mu f L} \sqrt{\frac{5^3}{3^5}} \\
Q_{req} &< \frac{0.717 H_0^3 F_A F_i \sigma \sin^2 \alpha}{3 \mu f L} N
\end{aligned}
$$

We are free to to increase N until this inequality is satisfied for any Q_{req}. This gives a minimum number of corners N_{min} with

$$N_{max} = \frac{3Q_{req}\mu f L}{0.717 H_0^3 F_A F_i \sigma \sin^2 \alpha}.$$ (2.22)

This calculation also requires that all geometrical and fluid parameters are identical for the N corners. We will also use the approximations for F_A and F_i used in (2.11) to better simplify the result.

$$N_{min} = \frac{21 Q_{req}\mu f L \cos(\alpha)}{0.717 H_0^3 \sigma \sin^3(\alpha)}$$ (2.23)

The most unrealistic assumption we've made here is that all the corner fill levels are exactly identical. If we want a safe average to to better estimate a safe number of corner it is reasonable that we require that small initial fill levels have large effects to our mean. Let us assume that for each index N, an initial fill level can be assigned to a given corner or $H_0(n)$ $n \in \{1, ..., N\}$. For a conservative estimate of M_{min} we suggest to simply use the $\texttt{min}(H_0(n))$.

3 Approximate Transient Analysis

The first dynamical problem addressed is sudden changes to flow rate in a corner δQ. This problem aims to describe disturbances to a steady state interior corner. This can arise in operation because of variations in a pump. We model this situation by assuming the initial condition is a steady state solution at some β_0. We assign different boundary heights instantaneously at $t = 0$ to some different β_f. Our analysis begins by solving the transient In order to find a time evolution solution, we use asymptotic methods. We utilize our generalized steady state expansion (2.9) to form an asymptotic series. This boundary height series reduces the problem to solving an infinite sequence of sub problems. By the grace of god, these problems are nothing but heat equations with constant boundary conditions and arbitrary source terms $S_{k,n}(z, t)$. The source terms cannot be determined, yet upper bounds are used to give estimates for the dynamics of sudden perturbations. The transients end up identical to the classical heat equation numerically and analytically.

3.1 The Start-Up Problem

The first transient problem we will solve is the *start-up* problem. This will model an interior corner that is initially flat with zero flow rate. When a pump is suddenly *started* a pressure gradient is imposed across the corner. These boundary pressures correspond to constant height boundary conditions. This disagreement between the
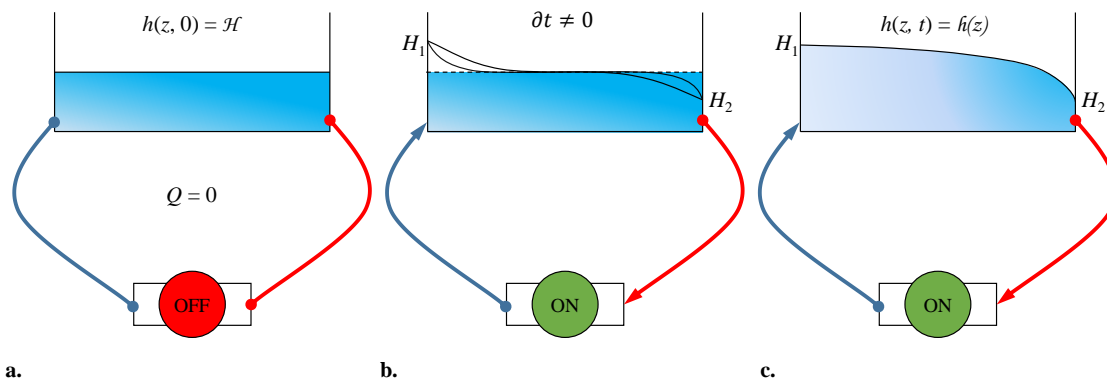
FIGURE 3.1: Three successive instances of time are shown during a *start-up* process. At first in image **a.** there is no pressure differential across the corner, the heights are equal an there is no flow rate. When the pump is turned on in part **b.** the boundary heights adjust instantaneously to H_1 and H_2. We seek a time constant τ that characterizes this decay to steady state depicted in part **c.**

boundary values and the initial condition introduces a transients we wish to study. At the start we are in grey analytical grounds. This is because the initial condition (2.6) satisfies (1.20), however it is *discontinuous*. In this simple instance we are save by White [42], where it is proven the solution is asymptotically stable. This means that any perturbation to an initial condition must decay to the analytical steady state. This however does not say anything about time dependent boundary conditions. For that we will introduce a model approximations nd investigate the error numerically. For now we will press along assuming we can still speak of *the* solution $h(z,t)$ to this problem. The expression in this section are non-dimensional are dimensionalized using tab 1.1. This solution reveals nothing profound as this time constant τ is identical what one gets from scaling. However the methods used provides a framework to solve much more complicated problems involving the corner. For now we will retain the constant volume assumption. Everything physically described is concisely formulated

as differential system,

$$\frac{\partial h^2}{\partial t} = \frac{\partial^2 h^3}{\partial z^2} \tag{3.1}$$

$$h(0, t) = H_1 \tag{3.2}$$

$$h(1, t) = H_2 \tag{3.3}$$

$$h(z, 0) = H_0 \tag{3.4}$$

We are still assuming volume conservation in the corner. This allows us to utilize our generalized steady state equation (2.9) found in chapter 2. To begin, we pose the naive asymptotic ansatz.

$$h(z, t) = \sum_{k=0}^{\infty} h_k(z, t) \phi^k \tag{3.5}$$

Our asymptotic parameter is no arbitrary small number but it is none other than $\phi = 1 - \beta$. This is why such great detail was made sin chapter 2 ensuring there was a method of approximately calculating $\beta(Q)$. To engineer flowrate is a given for which this parameter can be calculated. As long as the non-dimensional flowrate in the corner is small our inversion is valid as shown in Fig 2.4. Moreover, we have already seen that $\phi \approx 0$ represents slow flow rates. Each successive term represents a better approximation to slightly faster flow rates. Our results are not trivial either, any systems utilizing this interior corner flow will operate at small Reynolds numbers. This slow flow condition actually implies that a first order term solution is reasonably sufficient for modeling. But of course, what's the fun in just one.

3.2 An Asymptotic Solution

Asymptotic analysis require tedious calculations. This makes computer algebra systems a great tool. Everything is a consequence of substituting (3.5) into (3.1). After the algebra is carried out a new system of k heat equation determined. A critical step is the expansion of (2.9) about $\beta = 1$. This generate a sequences of numbers as shown in fig. 2.3 which fully define the boundary conditions for these k differential equations. We give the first 4 only to highlight an important pattern. The kth equation is $\mathcal{O}(\phi^k)$.

$$\frac{\partial h_0}{\partial t} = h_0 \frac{\partial^2 h_0}{\partial z^2} + 2\left(\frac{\partial h_0}{\partial z}\right)^2 \tag{3.6}$$

$$\frac{\partial h_1}{\partial t} = h_0 \frac{\partial^2 h_1}{\partial z^2} + 4\frac{\partial h_0}{\partial z}\frac{\partial h_1}{\partial z} + h_1 \frac{\partial^2 h_0}{\partial z^2} \tag{3.7}$$

$$\frac{\partial h_2}{\partial t} = h_0 \frac{\partial^2 h_2}{\partial z^2} + h_1 \frac{\partial^2 h_1}{\partial z^2} + 2\left(\frac{\partial h_1}{\partial z}\right)^2 + 4\frac{\partial h_0}{\partial z}\frac{\partial h_2}{\partial z} + h_2 \frac{\partial^2 h_0}{\partial z^2} \tag{3.8}$$

$$\frac{\partial h_3}{\partial t} = h_0 \frac{\partial^2 h_3}{\partial z^2} + \mathfrak{D}_3(h_0, h_1, h_2) \tag{3.9}$$

In (3.9), we have abstracted the remaining terms to a non-linear differential operator $\mathfrak{D}_k$. This operator couples all the previous solutions and only contains spatial derivatives. For the kth order equation this generic operator would couple all $k-1$ previous solutions $\mathfrak{D}_k(h_0, \ldots, h_{k-1})$. All the equations have associated boundary conditions and initial conditions.

$$h_0(0,t) = 0 \qquad h_0(1,t) = 0 \qquad h_0(z,0) = 1 \tag{3.10}$$

$$h_1(0,t) = \frac{1}{2} \qquad h_1(1,t) = -\frac{1}{2} \qquad h_1(z,0) = 0 \tag{3.11}$$

$$h_2(0,t) = \frac{1}{24} \qquad h_2(1,t) = -\frac{11}{24} \qquad h_2(z,0) = 0 \tag{3.12}$$

$h_0(z, 0) = 1$ only because of the initial condition for the given start-up problem we've described. It is important to realize that for all $k > 0$, all initial conditions $h_k(z, 0) \equiv 0$. This is only a specific instance though, an arbitrary initial condition function $h(z, 0) = f(z)$ would have many non zero polynomial terms for $k > 0$. We will try to address this at the end of this section.

We write out the kth boundary and initial conditions utilizing (2.15).

$$h_k(0, t) = A_k \qquad h_k(1, t) = B_k \qquad h_k(z, 0) = 0 \qquad (3.13)$$

Great simplification comes from solving the zeroth order equation. The equation (3.6) combined with (3.10) implies the constant solution $h_0 = 1$. Using (3.13) we write down the general system to solve for $k > 0$.

$$\frac{\partial h_k}{\partial t} = \frac{\partial^2 h_k}{\partial z^2} + \mathfrak{D}_k \qquad (3.14)$$

$$h_k(0, t) = A_k \qquad (3.15)$$

$$h_k(1, t) = B_k \qquad (3.16)$$

$$h_k(z, 0) = 0 \qquad (3.17)$$

The solution to (3.14) can be written down analytically. What we are doing is quite simply leveraging an existence and uniqueness proof for this system of equations [45, 46, 47]. It has been proven many times over that whatever function $\mathfrak{D}_k$ is, the solution exists and is unique. However, this is only true as long as $\mathfrak{D})k$ satisfy certain smoothness and continuity conditions, none of which are important for engineering purposes.

The solution is expressed as a fourier series with time varying coefficients $a_{k,n}(t)$.

$$h_k(z,t) = \sum_{n=1}^{\infty} a_{k,n}(t)\sin(n\pi z) \tag{3.18}$$

The coefficients are defined as

$$a_{k,n}(t) = \Gamma_{k,n} + \exp[-n^2\pi^2 t]S_{k,n}(t) \tag{3.19}$$

The term $\Gamma_{k,n}$ is the effect of the boundary condition to the solution and are defined as

$$\Gamma_{k,n} = \frac{2\phi^k}{n\pi}(A_k - (-1)^n B_k) \tag{3.20}$$

The much more indirect term is $S_{k,n}$. It represents all the non linear coupling of the previous solutions.

$$S_{k,n}(t) = \int_0^t \mathfrak{d}_{k,n}\exp[n^2\pi^2 t']dt' \tag{3.21}$$

with

$$\mathfrak{d}_{k,n} = 2\int_0^1 \mathfrak{D}_k \sin(n\pi z)dz. \tag{3.22}$$

One could argue that all we have done at this stage is push all the complexity into this $S_{k,n}$ term. However, (3.19) tells us that the coefficients decay to constants as $t \to \infty$ if $S_{k,n}$ is a bounded function. Further more we actually know that $S_{k,n}$ must be bounded precisely because of existence and uniqueness proofs for the solution to problem (3.1).

3.2.1 $\mathcal{O}(\phi)$ Solution

With out any approximation we can write down the first order solution. We substitute $h_0 = 1$ into (3.7). In the general framework $\mathfrak{D}_1 = 0$. This simplifies it to a linear heat equation.

$$\frac{\partial h_1}{\partial t} = \frac{\partial^2 h_1}{\partial z^2}$$
$$h_1(0, t) = \frac{1}{2}$$
$$h_1(1, t) = -\frac{1}{2}$$
$$h_1(z, 0) = 0$$

Which has the solution,

$$h_1(z, t) = \frac{1}{2} - z - \sum_{n=1}^{\infty} \frac{(1 + (-1)^n)}{n\pi} \exp[-n^2\pi^2 t] \sin(n\pi z) \tag{3.23}$$

Remember all this work was to only derive the solution's functional form. We set out to determine time constants for the evolution. We re-dimensionalize for the time constant of first order perturbations,

$$\tau_1 = \frac{\mu f L^2}{4\pi^2 \mathcal{H}\sigma \sin^2 \alpha}. \tag{3.24}$$

We have then learned two things from this analysis. One is the additional scaling factor of $4/pi^2$, the other is the that a linearization of the governing equation for the start up problem possesses a completely analytical solution. This is the only difference from the time constant found from a simple scale balance. For *volume*

44

conserving interior corners the transients for sudden disturbances is (3.24). This is remarkably true even for $\phi \to 1$, which the purpose of the next calculations. We plot a comparison to a numerical solution in figure 3.2.

3.2.2 $\mathcal{O}(\phi^2)$ Solution

For the second order solution we must make some approximation assumption to arrive at something we can write down. We substitute $h_0 = 1$ into (3.8). The constant boundary conditions $\{A_k, B_k\}$ are found from Mathematica. Many terms zero out because of $h_0 = 1$. The second order differential system to solve is,

$$\frac{\partial h_2}{\partial t} = \frac{\partial^2 h_2}{\partial z^2} + \mathfrak{D}_2(h_1) \tag{3.25}$$

$$h_2(0, 1) = \frac{1}{24} \tag{3.26}$$

$$h_2(1, t) = \frac{-11}{24} \tag{3.27}$$

$$h_2(z, 0) = 0. \tag{3.28}$$

Here we see the first simplification of $h_0 = 1$. It makes the differential operator $\mathfrak{D}_2$ not a function of h_0. This isn't the simplest forcing functions for the heat equation but a forcing function it is. There are subtle convergence mathematics that go into proving such a function is well defined even. We will simply blaze along assuming whatever has to be assumed is. In the end we are comparing to a numerical solution to see if any of our methodologies hold any water.

$$\mathfrak{D}_2(h_1) = h_1 \frac{\partial^2 h_1}{\partial z^2} + 2\left(\frac{\partial h_1}{\partial z}\right)^2. \tag{3.29}$$

Recall that h_1 was an infinite series itself. To the mathematician this operation may well not be defined. For the engineer, ignorance is bliss. In order to obtain higher order solutions we will make use of the existence of the solution itself. We are going to *construct* a series solution based on certain properties of (2.9) and (3.29). We require that the kth steady-state solution must be equal to the $p_k(z)$ found in (2.14). This allows us to solve for the limiting case of $\mathfrak{D}_2$.

$$0 = \frac{\partial^2 h_2}{\partial z^2} + \lim_{t \to \infty} \mathfrak{D}_2$$

$$-\lim_{t \to \infty} \mathfrak{D}_2 = \frac{\partial^2 h_2}{\partial z^2}$$

$$= \frac{\partial^2 p_2}{\partial z^2}$$

$$= \frac{\partial^2}{\partial z^2}(-z^2 + \frac{1}{2}z + \frac{1}{24})$$

$$\lim_{t \to \infty} \mathfrak{D}_2 = 2$$

The second consideration is how quickly does this forcing function limit to its steady state value. Here is where we make a rough estimate based on (3.29). Considering the scales of (3.29) and utilizing our time scale (3.24),

$$\mathfrak{D}_2 \sim \frac{h_1^2}{L^2},$$

$$\sim \frac{\exp[-t/\tau_1]^2}{L^2},$$

$$\sim \frac{\exp[-2t/\tau_1]}{L^2}.$$

This short scale argument tells us that the $\mathfrak{D}_2$ forcing function reaches its steady state *twice* as fast as the other differential terms. The higher order $\mathfrak{D}_k$ by the same
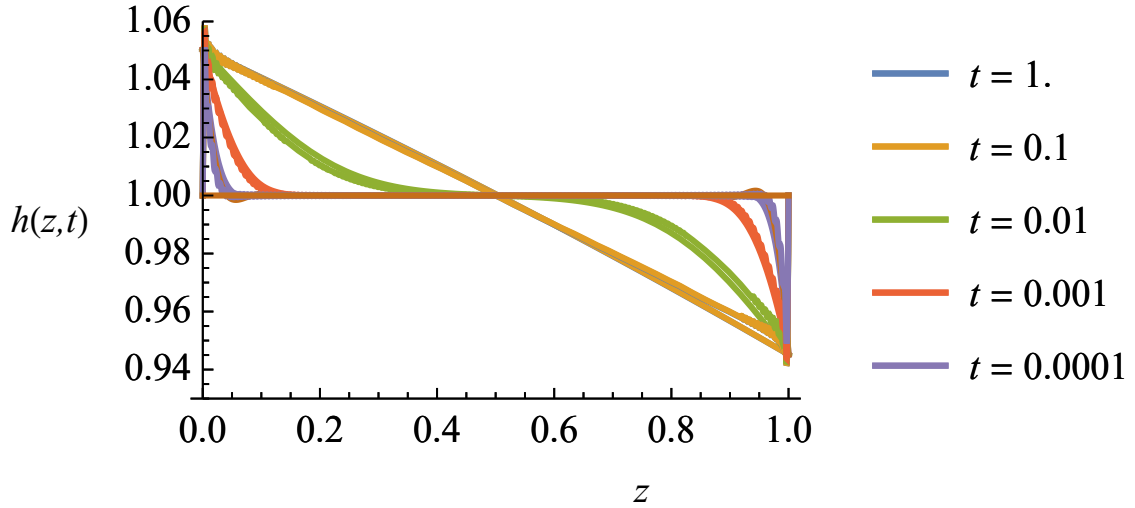
FIGURE 3.2: Slow transients with $\phi = 0.1$

arguments decay like $\mathfrak{D}_k \sim \exp[-2kt]$. This gives good reason to *approximate* the coupling term as its steady state function. This makes a much more solvable heat equation system. We compare the numerical and analytical solution in figure 3.3. Calculating this infinite series solution is actually slower than numerically solving it. This solution required 300 terms of both series to best approximate the spatial distribution. However the purpose is to demonstrate how the decay rate even for large values of β is eq (3.24). We can push this method further for flow rates approaching the maximum, $\beta \to 0$. Moreover, this method of approximating a complicated coupling term could prove useful for other nonlinear problems. We push this method for flow rates approaching the maximum, $\beta \to 0.5$. The comparison of the analytical and numerical is given in figure 3.4.

47
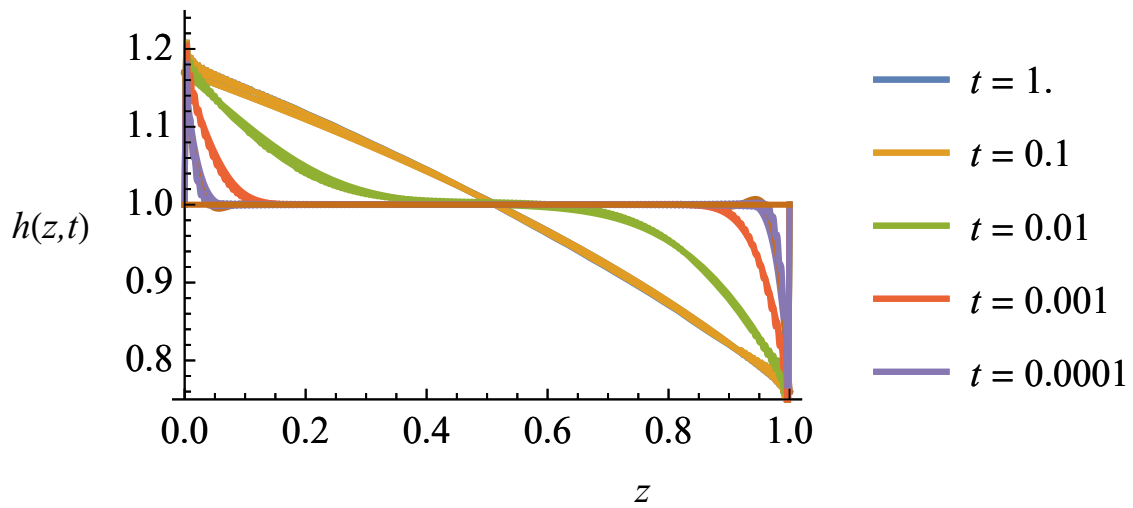
FIGURE 3.3: Medium transients with $\phi = 0.35$
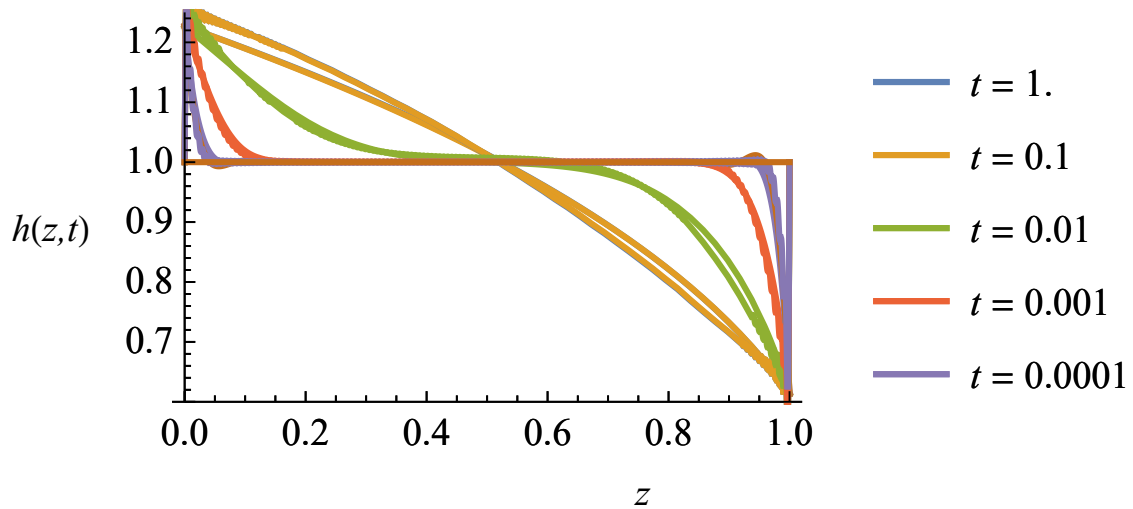
FIGURE 3.4: Large transients with $\phi = 0.5$

3.2.3 $\mathcal{O}(\phi^k)$ Solution

We now can lay out the program to construct the kth order solution. This is not completely analytical as is requires software to calculate the $p_k(z)$ coefficient functions. First we calculate $\mathfrak{D}_k$ using $p_k(z)$.

$$\mathfrak{D}_k = -p_k(z)'' \tag{3.30}$$

Now the system is solved as it can be put in the form of (3.18) using (3.19), (3.20), (3.22), and (3.21). We now see just how powerful (2.14) is. The coefficient polynomial functions $p_k(z)$ do a number of things. It helps formulate an infinite sequence of solvable problems. It calculates A_k. It calculates B_k. It approximates nonlinear coupling function $\mathfrak{D}_k$ It has allowed us to *construct* a solution.

3.2.4 Steady-State Initial Condition $f(z) = h_s(z; \beta_0)$

We extend our methods to develop transients to address perturbations between two distinct steady state solutions. We can investigate closely into quasi-steady dynamics this way. Let us say that the flowrate in the corner is some function of time $Q(t)$, and at a given time t_0 the system is at a steady state defined by (2.9). This is to say $h(z, t_0) \equiv h_s(z; \beta(Q(t_0)))$. We can simply think of $\beta_0 \equiv \beta(Q(t_0))$. Since t_0 is just a reference time value we set it to zero and just think of time progressing forwards from this point. Now we look at a sudden jump from a flowrate defined by $\beta(Q(t_0)) \mapsto \beta(Q(t_0 + \delta t))$. The steady state functions are identified by an initial flow at β_0 which is suddenly jumped to a new flow rate β. Staying in the framework set

in section 1.4 the initial condition for this model is,

$$h(z,0) = f(z) \equiv \begin{cases} H_1 & z = 0 \\ h_s(z, \beta_0) & 0 < z < 1 \\ H_2 & z = 1 \end{cases} \tag{3.31}$$

The start-up problem is actually a special case of this problem with $\beta_0 = 1$. We apply the same expansion methods used in the start-up problem. This function has its own taylor series now in the variable β_0 or equivalently $\phi_0 = 1 - \beta_0$.

$$f(z) = \sum_{k=0}^{\infty} p_k(z)\phi_0^k \tag{3.32}$$

There are now two competing parameters which we are assuming we know, where we start ϕ_0, and where we end ϕ. This requires algebraic manipulation of (3.32).

$$\begin{aligned} f(z) &= \sum_{k=0}^{\infty} p_k(z)(\frac{\phi}{\phi})^k\phi_0^k \\ &= \sum_{k=0}^{\infty} p_k(z)(\frac{\phi_0}{\phi})^k\phi^k \\ &= \sum_{k=0}^{\infty} \Phi^k p_k(z)\phi^k \end{aligned} \tag{3.33}$$

This new ratio Φ is a measure of the difference between the steady states. These step have been taken in order to make expansions all in terms of the *same* parameter ϕ. This is so we can keep our asymptotic assumption (3.5). The only difference to so far is some relaxation on the initial condition. Following the same arguments and

process of section 3.1, we have new initial conditions for the k^{textth} sub problem as,

$$h_k(z, 0) = \Phi^k p_k(z). \tag{3.34}$$

The time varying fourier coefficients functions $a_{k,n}(t)$ now have an additional term.

$$a_{k,n}(0) = 2\Phi^k \int_0^1 p_k(z) \sin(n\pi z) dz. \tag{3.35}$$

This term represents the initial condition effect on the solution. The new coefficients function can be expressed as three distinct terms. We can reuse the definitions for (3.20) and (3.21)

$$a_{k,n}(t) = \Gamma_{k,n} + \exp[-n^2\pi^2 t]\{a_{k,n}(0) + S_{k,n}(t)\} \tag{3.36}$$

The first term is out boundary term that ensures the solution decays to the steady state prescribed by A_k, B_k. The second term is the initial condition term which is simply the fourier expansion of each $p_k(z)$. The third term is effect of the nonlinear coupling of all k solutions in $\mathfrak{D}_k$. This general solution agrees with the start-up problem when $f(z) = 1$, which simply makes $a_{k,n}(t) = 0$ for $k > 0$.

3.3 Time Dependent Boundary Conditions

The most un-physical assumption so far is this *instantaneous* shift in boundary values. We now analyze boundaries which are functions of time $\{H_1(t), H_2(t)\}$. We will require some basic functional assumptions on these boundary functions. The derivative of the boundary is a velocity in the y direction. In order to arrive at our

51

governing equation this velocity scaled with the z velocity as $V_0 \sim \epsilon W_0$. However, the boundaries could be much slower than this estimate since

$$\left|\frac{dH_i}{dt}\right| = V_0 < \epsilon W_0. \tag{3.37}$$

Where $i = \{1, 2\}$ in the above expression. Practical functions to assign to the boundaries could be periodic or exponential. For periodic boundaries one could model a *peristaltic* pump used to circulate fluid with $H_i \sim A \sin(\omega t + \psi)$.. An exponential function models a slow approach a constant value, $H_i \sim A + B(1 - \exp[t/\tau])$. This fixes the pesky "instantaneous" shift of the boundary values from the initial condition in the start-up formulation. We first begin with a scale analysis on the impact these boundary functions have on solutions. We search for an *influence length* ℓ and a boundary time scale τ_b. Previously we scaled h with a representative height H_0 calculated from the the initial condition using (2.7). The *boundary* time scale is calculated to be

$$\tau_B \sim \frac{H_0}{V_0}. \tag{3.38}$$

In this time scale we do not use the length of the corner as we are considering the time scale of up and down motion in the corner. We insert these time scales into the governing equation to find ℓ is

$$\ell = \sqrt{\frac{F_i H_0^2 W_0}{3 V_0}}. \tag{3.39}$$

The boundary effects are inversely proportional to the boundary velocity. If the boundary velocity is on the same order as the characteristic velocity, then the influence

length is proportional to the height of the corner H_0. With this concept we see that for very slow boundary velocities the influence length extends into the entire solution domain. In the original formulation recall our governing scales had $V \sim \epsilon W_0$. This is the maximum boundary velocity our model can handle before inertial effects must be considered. We use a standard approximation $F_i = 1/7$ to see the maximum influence length at the boundaries is,

$$\ell \leq \frac{H_0}{\sqrt{21\epsilon}}. \tag{3.40}$$

We already know then that the boundary velocities must be slow but how slow is different question. To answer this we introduce a parameter a. We express the boundary velocities as $V_0 = \epsilon^a W_0$, with $a \geq 1$. This allows us to split the effects of time varying boundaries into simpler cases involving an analysis on a. We restrict $a < 1$ because in this case $V \gg W_0$, and all the assumptions used to derive the governing equation are violated. Specifically, this means our velocity scaling was incorrect as the dominate velocity would be up and down in the corner. This analysis would require a full 3D analysis, this is a very interesting new path for this type of flow and readers are encouraged to tackle such an applicable problem.

When we use the boundary time scale $t \sim 3L/F_i V_0$ the new non-dimensional governing equation is

$$\frac{\partial h^2}{\partial t} = \epsilon^{2-a} \frac{\partial^2 h^3}{\partial z^2}. \tag{3.41}$$

The governing equation in this form shows a dependence on the boundary velocity with the parameter a.

Quasi-Steady $a \gg 1$

The first approximation we make are for very slow boundary functions. This is a limiting case for when boundaries are weak functions of time. These are *quasi-steady flows*. The solution is expressed in terms of the time dependant boundary functions $H_1(t), H_2(t)$.

$$h(z,t) = H_1(t)(1 - (1 - \beta(t)^3)z)^{1/3} \tag{3.42}$$

We keep the same definition of β only now it is a function of time. This solution does not require volume conservation either. However, eq. (3.42) will be our main equation used to formulate the dynamics of average meniscus height in chapter 4.

Transient Boundaries $a \sim 2$

There is a case when the boundary variations are on the same time scale as the governing equations. This is really a fully dynamics problem and forces us into strange new territory to approximate the transients. At this stage we will introduce inspired by a new technique inspired by [27]. We refer to this technique as *model-approximation*. We will simply alter the governing equation to yield analytical results. This method is contentious, however we are confident in its accuracy by comparing it to stable numerical solutions. We also are hinted a remarkable heat equation similarity based on reoccurring transients in all the asymptotic analysis. It is quite stunning how accurate an approximation this is when we compare numerical and analytical solution surfaces with a relative error metric. We preface that we have no theory or proof that such a method like this is general.

We are motivated by addressing the real non-linearity of our governing equation, a mismatch of exponents. Let us revisit the original initial boundary value problem

to solve. In our rescaling we assume that $a \sim 2$. This means that $\epsilon^{2-a} = \eta' \sim \mathcal{O}(1)$
Keep in mind that unless the corner is fully pinned this means our model is only valid
for $0 < h(z,t) < H_0$.

$$\frac{\partial h^2}{\partial t} = \eta' \frac{\partial h^3}{\partial z^2}, \tag{3.43}$$

$$h(0,t) = H_1(t) \tag{3.44}$$

$$h(1,t) = H_2(t) \tag{3.45}$$

$$h(z,0) = f(z) \tag{3.46}$$

If the governing equation was instead,

$$\frac{\partial \tilde{h}^3}{\partial t} = \eta \frac{\partial \tilde{h}^3}{\partial z^2}, \tag{3.47}$$

$$\tilde{h}^3(0,t) = H_1^3(t) \tag{3.48}$$

$$\tilde{h}^3(1,t) = H_2^3(t) \tag{3.49}$$

$$\tilde{h}^3(z,0) = f^3(z), \tag{3.50}$$

we would have an infinite fourier series solution with time varying fourier coefficients.
The solution would come from a defining $u = \tilde{h}^3$ and solving the differential system
using Fourier Series. The solution is,

$$u(z,t) = \sum_{n=0}^{\infty} a_n(t) \sin n\pi z, \tag{3.51}$$

where $a_n(t)$ are solutions to n ordinary differential equations,

$$\frac{da_n}{dt} + \eta\lambda_n a_n = \eta 2n\pi(H_1^3(t) - (-1)^n H_2^2(t)) \tag{3.52}$$

$$a_n(0) = 2\int_0^1 f^3(z)\sin n\pi z\, dz. \tag{3.53}$$

The main question is then: How similar is $\tilde{h}$ is to $h(z,t)$?

This is the purpose of this final section and will be a reoccurring theme throughout this entire thesis. We have introduced a parameter η to the right hand side of the equation as an "analytical" fitting parameter. We are motivated to do this as we have altered the power on the left hand side of the differential equation, so something heuristically must be adjusted on the right. We compare the numerical solutions of both systems of equations and the analytical series solution. (3.51). The results are seen in fig. 3.5 and fig. 3.6. It is remarkable how well the approximation is when we select $\eta = 4$. This choice of $\eta = 4$ was done only with a manual bisection method selecting integers. There certainly is room for an optimum selection of η in the future. We present only our findings for this approximation methods that seems almost too good to be true. In table xx, we present the error between the two solutions using $\eta = 4$ and do a parameter sweep of boundary time scales. The initial condition becomes less important as time grows which again verifies the recent stability proof [42].

For a comparison we need to define a class of boundary functions. We are motivated by applications of the proposed system and select cyclical functions modeling

peristaltic pump frequencies. Our general class of boundary function as then,

$$H_1(t) = A\sin(\omega_1 t) + H(0), \tag{3.54}$$

$$H_2(t) = B\sin(\omega_2 t) + H(1). \tag{3.55}$$

Our parameter sweep is done for $0 < A, B < 0.3$, $0 < \omega_1, \omega_2 < 100$ The amplitudes are bounded by $A, B < 0.3$ in order to ensure that $h(z,t) > 0$ for $t > 0$. Notice our class of boundary function is constructed so that $h(0,0) = H_1(0) \equiv H(0)$ and $h(1,0) = H_2(0) \equiv H(1)$. This is a continuity condition which allows us to assume a solution exists and is unique. This is not an unreasonable assumption since, at least in my experience, I have never seen a liquid in two places at the same time. This importantly allows us to leverage the existence and uniqueness proof [44]. We are only interested in real positive solutions $0 < h(z,t) \in \mathbb{R}$. This means even though we are considering $\tilde{h} = u^{1/3}$, we know the other two solutions of this root are complex. This means the inversion is one to one and valid for our purposes.

We must assume an initial condition at this stage in order to calculate anything. This assumption is interesting and certainly a subject of further analysis. A rigorous mathematical question would be to see if there exists from $f(z)$ such that the solution to eq. (3.43) diverges as $t \to \infty$. We will not worry about this detail as the results are striking enough to present alone. We will use a simple constant initial condition used in section 3.1. This is a general enough assumption, because we are more concerned with the agreement of the solutions as time marches on and the initial conditions becomes nothing but a memory. For a numerical simulation we will set $T = 1000$.

Given these assumption we have reduced the dimensional enough to populate a

relative error surface. Our independent variables will be the ratio of the frequencies and amplitudes $\mathcal{A} = A/B, \Omega = \omega_1/\omega_2$. We also plot in fig. (3.6) an error surface with a maximum relative error defined as

$$\Delta(\mathcal{A}, \Omega) = \max \frac{|\tilde{h}(z,t) - h(z,t)|}{h(z,t)} \quad t \in [0, T) \quad z \in [0, 1] \qquad (3.56)$$

There are two ways to calculate $\tilde{h}(z,t)$. One is to compute a partial sum of (3.51), or to compute a numerical solution to $u(z,t)$ and then compute $u^{1/3}$. We provide both simply to show agreement converges in both cases. This is shown in Fig. 3.6 and notice that the relative error is under 5% for the analytical $\tilde{h}$ and numerical. A full parameter sweep table is far too large to include in a document, however a full numerical investigation has been made mapping out this entire parameter space. The data can be downloaded at,

$$\texttt{https://github.com/smohler/thesis/.../error.csv}$$

and investigated further. The main conclusion is that never once in this parameter sweep did relative error grow beyond %5. I myself was truly surprised by this given the ad-hoc nature of selecting $\eta = 4$
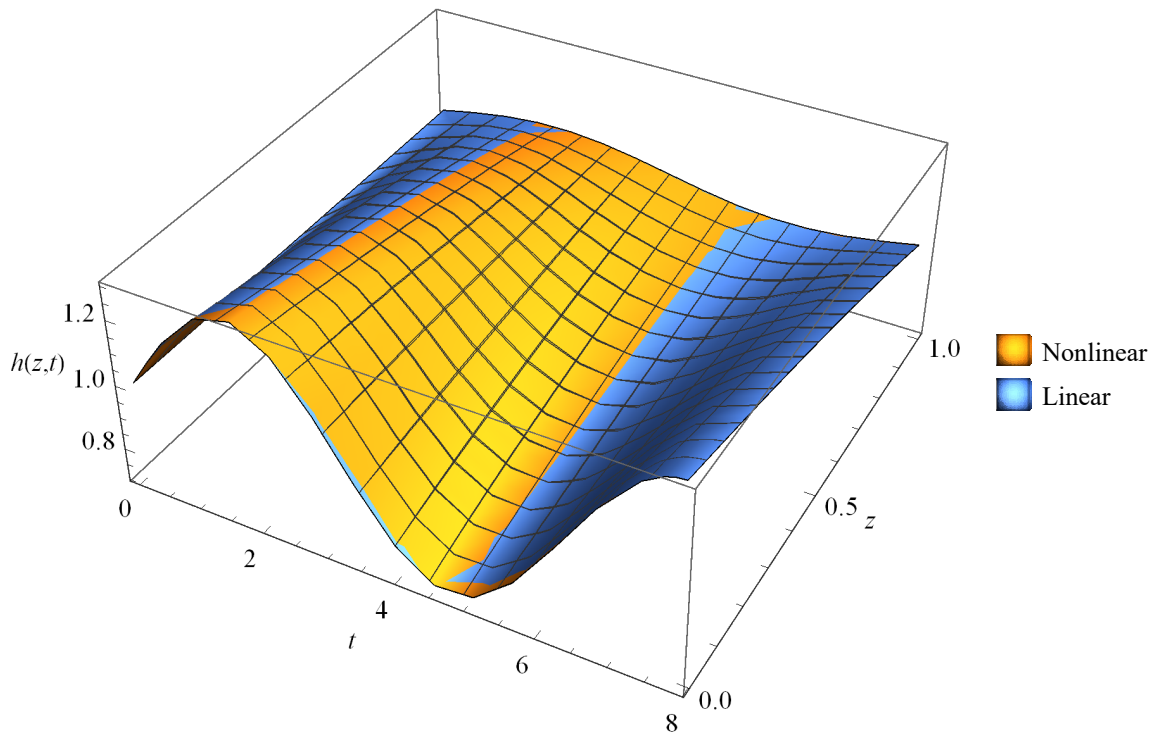
FIGURE 3.5: A comparison of the solution surfaces with parameters $A = 0.3$, $B = 0.05$, $\omega_1 = 1$, $\omega_2 = 0.8$. Graphically the surfaces are coincident even though the $\tilde{h}(z,t)$ is the solution to a linear equation. The analytical solution for the linear case here is using $N = 300$ terms of the Fourier Series. The numerical integration tolerance is set at the default values in `Mathematica`. For an entire parameter sweep the surfaces resemble this, so this example is an illustration of how well this approximation works
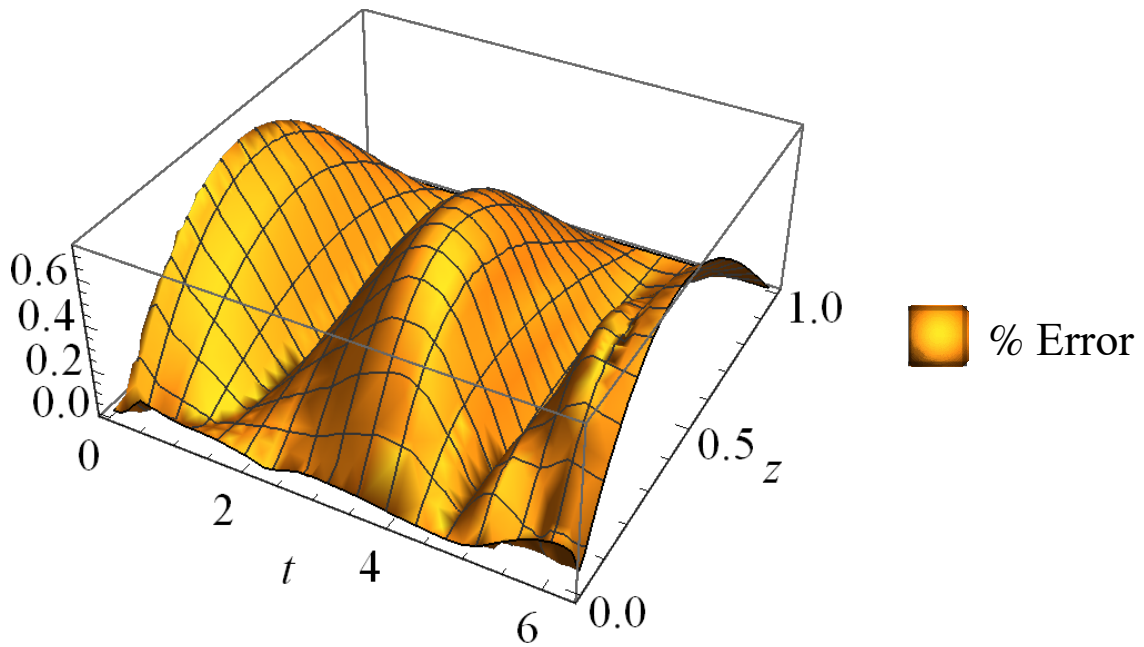
FIGURE 3.6: The relative error between the solutions surface in Fig. 3.51. This particular case is quite low but shares a common theme of this approximations. Most of the error is in the middle of the domain about $z \approx 0.5$. As we move closer to the boundaries the errors decays to zero. This error surface continues like this even for $t \to 1000$, which suggest that a stable approximation is achieved with this method.

4 Average Height Dynamics

The capacitance is an open channel's ability to store volume. Until now our analysis has been limited by assuming constant volume in the corner. In a real system of parallel channels, the corners exchange fluid volume with each other. For instance, if one channel were to become instantly blocked the volume of that corner would be distributed to the others channels. This distribution would be seen as an increase in the average height along the corner $\bar{H}$. We derive a nonlinear differential equation that governs the balance of flowrate thru and filling of a channel. Several assumptions must be met to satisfy this equation and they are developed herein. This evolution equation serves the model function for the capacitor term in a circuit network idealization. An implicit integral solution is found and an approximations are made. The solution behavior is dependent on the initial condition and boundary conditions of the corner. It is determined that as time approaches infinity or if the initial profile and steady state profile are approximately the same the solution behaves as an exponential. This agrees with the analysis made so far when volume is conserved. If the initial average height is far away from the steady state average height and the corner is *draining*, the solution behaves with a power law $\bar{H} \sim t^{-k}$ when $t = 0$, but still converges to an exponential as $t \to \infty$. Finally if initial average height is far away from the steady state average but the corner is *filling*, the solution can be approximated as a cube root of an exponential function.

4.1 Average Meniscus Height

We are concerned with the volume drain or gain in a corner which means we seek to understand the dynamics of volume in the corner V(t). At this point we focus on a single corner. Until this point we have assumed that volume is conserved in a single corner $V'(t) \equiv 0$. We are now ready to relax this assumption. First we will define an average meniscus height to be the root mean square of the integrated domain. This assigns a single height value $H(t)$ given a meniscus profile function $h(z, t)$.

$$H(t) = \left(\int_0^1 h(z, t)^2 \mathrm{d}z \right)^{1/2}. \tag{4.1}$$

With this definition we can now consider the volume dynamics in terms of average meniscus height via,

$$\frac{dV}{dt} = \frac{d}{dt} \int_0^1 h(z, t)^2 \mathrm{d}z = \frac{dH^2}{dt}. \tag{4.2}$$

To formulate a tractable model we first assume the existence of a steady state solution. This means when it comes to corner accumulating or draining from a corner an equilibrium is reached and

$$\lim_{t \to \infty} H(t) = H_\infty. \tag{4.3}$$

This is a delicate assumption. We are a-priori assuming that given set corners with an arbitrary distribution of initial fill levels, the system attains a steady state where all the corners reach an equilibrium fill level H_∞. This fill level is attributed to the steady state flow-rate thru the corner. This is analogous to our original *start-up* problem but now we have a parallel problem. Figure 4.1 is a schematic of such a process. At $t = 0$ we have a system with many flat meniscus profiles all filled at different height

values $H_i(0) = \mathcal{H}_i$, where $i = 1, 2, \ldots N$. These define N initial conditions to assigned to the N nonlinear partial differential equations governing each individual corner. At this stage we will still only focus on a single corner and drop the subscript i. The major analysis is on the process of volume draining or gaining in the corner due to an imbalance of flowrate in and out of the corner. The next question is what *boundary* conditions do we assign to these N differential equations? This is the boundary value problem which complicates all the matter.

If we knew exactly what the flowrate was in each corner at any instant in time we could close this problem. One first approximation is to assume that a constant flowrate is *instantaneously* imposed on every corner when $t > 0$. This amounts to constant height values at the inlet and outlet of each corner. This process is just as physical as our original start-up formulation discussed in 3, but unlike a single *volume conserving* we can now have two cases for boundary heights. The first is volume drain when $H_2 < H_1 < H_0$, the second is volume gain when $H_0 < H_2 < H_1$. We will ignore cases when $H_1 < H_2$ as this is just the reversed flow situation.

In fig. 4.1a. we illustrate this process of instantaneously imposed boundary values, and in fig 4.1c. we depict the steady state meniscus profile in every corner. This is where all interior corner settle down to some calculated H_∞. The murky waters lay in the transients sketched in fig 4.1b. A major simplification comes from the realization that instantaneously boundary conditions should be ignore entirely. The reason being the solution can only model volume dynamics with opposing flowrate directions. This is impossible as flowrate will always be left to right in these corners. Volume is really *accumulated* from flowrate imbalance at the ends of the corner which slowly raise or lower. Thinking back to sec 3.3 this is the the quasi-steady case when $a \gg 1$. This

63
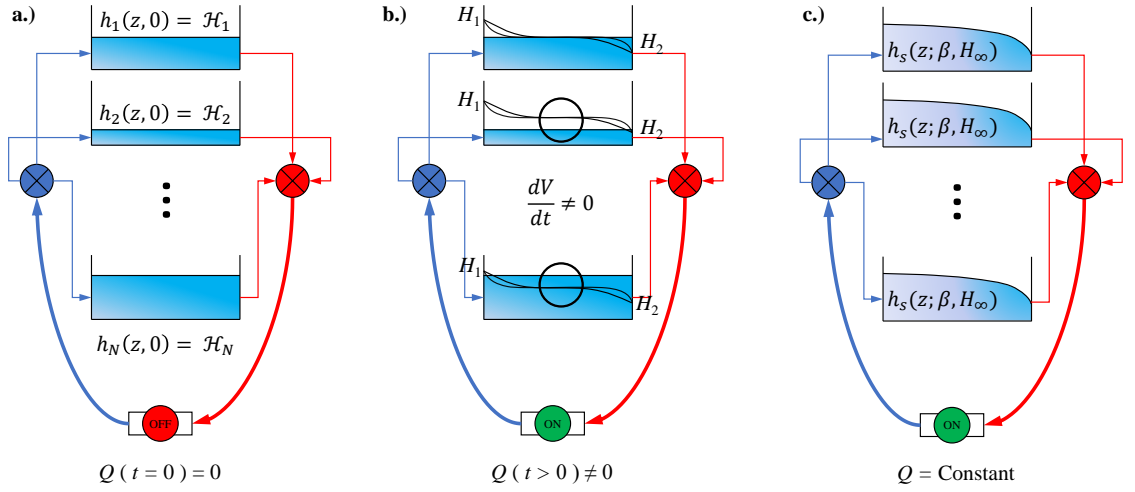
FIGURE 4.1: An illustration of the *parallel* start-up problem analogy. In **a.** all corners are filled to some arbitrary level, they are free to be greater or less than steady state fill level H_∞ seen in **c.**. In **b.** we sketch how volume is *not* conserved in a single corner.

motivates us to analyze volume dynamics in a corner as a quasi-steady process. This allows us to port over the results of chapter 2 to investigate volume dynamics.

4.2 Quasi-Steady Volume Exchange

The assumption of quasi-steady manifests itself with very slow moving boundaries. Even with this Quasi-Steady assumption this means that the flow speed parameter is a function of time $\beta(t)$. We would like to disjunct this assumption and say β is a constant function. The following discussion is heuristic argument that this is valid.

Initially when $t = 0$ we will assume a flat meniscus height of $\mathcal{H}$ with $\beta(0) = 1$. In the end we also are assuming that a slow flowrate is reached so similar to (4.3) we

say,

$$\lim_{t \to \infty} \beta(t) = 1 - \epsilon \equiv \phi_0, \tag{4.4}$$

and $\varepsilon \ll 1$. We have kept the same asymptotic parameter ϕ that was used heavily in chapter 3. It is important to remember that given a small value of Q we have a means to calculate ϕ_0.

Since we are assuming equilibrium is eventually met with (4.3), we model these boundary functions $\{H_1(t/\tau_1), H_2(t/\tau_2)\}$ with just barely different time constants $\tau_1 \approx \tau_2 \gg 1$. We require that in the limit of these functions,

$$\lim_{t \to \infty} H_1(t/\tau_1) = H_\infty(1 + \varepsilon_1), \tag{4.5}$$

$$\lim_{t \to \infty} H_2(t/\tau_2) = H_\infty(1 - \varepsilon_2). \tag{4.6}$$

where $i = 1, 2$, and $0 < \varepsilon_i \ll 1$. Notice in the limits that $H_2 < H_1$ and furthermore,

$$\phi_0 = \frac{1 - \varepsilon_2}{1 + \varepsilon_1} \approx 1. \tag{4.7}$$

We next look at the transients of $\beta(t)$, letting superscript $(') = d/dt$ and taking the derivative we find

$$\frac{d\beta}{dt} = \frac{\dfrac{H_2 H_1'}{\tau_2} - \dfrac{H_1 H_2'}{\tau_1}}{H_2^2}. \tag{4.8}$$

We now need derivative information on the boundary functions $H_i'(t)$. This comes from the original scaling of the equations, recall that $v_0 \sim \epsilon w_0$, and therefore $H_1' \sim H_2' \sim \epsilon w_0$. With this final scale a *necessary condition* for when we can say $\beta'(t) \approx 0$

is

$$H_2^2 \gg \epsilon w_0 \left(\frac{H_2}{\tau_2} - \frac{H_1}{\tau_1} \right) \approx 0. \tag{4.9}$$

A sufficient condition would be,

$$\frac{H_2}{\tau_2} = \frac{H_1}{\tau_1}. \tag{4.10}$$

Which means that not only do we need the time constants for the boundaries to be large, but they indeed must be similar with $\tau_2 \approx \tau_1$. With (4.10) we may approximate $\beta(t) \approx \phi_0$.

This allows for flowrate to be calculating using (2.9). We calculate flowrate of quasi-steady flows using the generalized steady state equation (2.9).

$$Q(\phi_0, H(t)) = -H(t)^3 \Gamma(\phi_0) \tag{4.11}$$

$$\Gamma(\beta) = \left(\frac{5^3}{3^5} \frac{(1 - \beta^3)^5}{(1 - \beta^5)^3} \right)^{1/2} \tag{4.12}$$

This expression now lets us analyze the dynamics of this average fill height $H(t)$. For a large parallel system, fundamentally flow is split up from an initial source Q_{tot}. The simplest assumption is that for N corners, the flow is *equally* distributed amongst all the corners at steady state. This means for a single corner in a parallel network the steady state flowrate thru it becomes

$$\lim_{t \to \infty} Q(\beta(t), H(t)) = \frac{Q_{tot}}{N}. \tag{4.13}$$

We should note that a much more advanced analysis could be made with two more refinements. One is to allow a more complicated *distribution* of flowrate in the corners. A general approach would be to model the distribution with a *partition of unity* such

66

that,

$$Q_{tot}(t) = \sum_{i=1}^{N} \phi_i(t) Q_{tot}(t). \tag{4.14}$$

Notice that (4.13) is a specific case of (4.14) where $\phi_i(t) = 1/N$.

Let us now set a constant flow speed $\beta = \phi_0$ such that (4.10) holds. This simply means that $1 - \varepsilon < \phi_0 < 1$ where $\varepsilon = \varepsilon_2/(1 + \varepsilon_1)$ We assume that we have a set of corner all with an initial fill level $H(0)$. Recall we have dropped indices for now as we are still only analyzing one single corner. At this stage we already can make a bulk prediction of the volume dynamics.

Case 1: Volume Gain, $\qquad \dfrac{Q_{tot}}{N} > Q(\phi_0, H(0)),$

Case 2: Volume Drain, $\qquad 0 < \dfrac{Q_{tot}}{N} \leq Q(\phi_0, H(0))$

The real power of all the assumptions made with (4.10), (4.13), and (4.3), is we can now *calculate* H_∞ to be

$$H_\infty = \left(\frac{Q_{tot}}{N}\right)^{1/3} \frac{1}{\Gamma(\phi_0)}. \tag{4.15}$$

The power of (4.15) is that we have developed a set of assumptions that inform us about the initial state and final state of a corner. We can calculate the boundary heights in the final state using our generalized steady state solution (2.9)

$$H_1 = \hbar(0; \phi_0, H_\infty) \tag{4.16}$$

$$H_2 = \hbar(1; \phi_0, H_\infty) \tag{4.17}$$

We should remark that while we are using ϕ_0 as an independent variable it really

is dependent on *flow rate*. This illustrates even more the usefulness of (2.19). An example situation would go as follows. A flowrate Q_{tot} is set by an engineering requirement. Given corner dimensions and fluid properties Q_{tot} is then subdivided into a design corner count N. This calculation is made explicit with (2.23). Next a ϕ_0 is calculated after q_i is non-dimensionalize by Aw_0 using (2.19). We also should note that we can always satisfy $q_i \ll 1$ simply by adding more corners into such a parallel system. This means given a flowrate in the corner $q_i = Q_{tot}/N \ll 1$, we can determine $\phi_0, H_\infty, H_1, H_2$.

4.3   Governing Nonlinear ODE

We will now develop a dynamical model of the volume transient in a corner. Our model is *highly* restrictive given the assumptions developed so far. However, we make the case that this is at least a starting point for more detailed investigations. If *a* solution can be found there is always hope that more complicated solutions can transform in some fashion to it, so our efforts are not completely in vein. Our model begins with a small change in volume dV in a corner. Instead of considering a small positive change in time dt we will use a *negative* difference $-$dt. We do this because we already know the end state of this model and are only interested in the dynamics of getting from initial to final state.

$$\mathrm{d}V = Q(\phi_0, H_\infty)(-\mathrm{d}t) - Q(\phi_0, H(t)(-\mathrm{d}t) \tag{4.18}$$

We non-dimensionalize this equation with the following scales:

$$H' \sim H_0 \qquad\qquad t' \sim 3L/F_i W_0 \Gamma(\phi_0). \tag{4.19}$$

Here ($'$) refers to a dimensional quantity. We also define new parameter $\gamma = H_\infty/H_0 \in (0,\infty)$ which is analogous to β. It is a non-dimensional number which measures the *intensity* of flow rate. The difference between β and γ, is that β measures the axial flow intensity while γ measures the cross-sectional flow intensity. Again, similar to β when $\gamma \approx 1$ we have very little flow. When $H_0 \to 0$ we have a very shallow corner and $\gamma \to \infty$. There is an interesting consequence of this which we can see from the implicit solution of (4.20). The dimensionless governing equation becomes,

$$\frac{dH^2}{dt} + H^3 = \gamma^3, \tag{4.20}$$

$$H(0) = 1. \tag{4.21}$$

The right hand side of (4.20) is a *constant* value of γ for this parallel start-up problem. This comes from assigning *constant* boundary conditions to the original partial differential equation. Similarly initial condition (4.21) originates from a root-mean-square of the partial differential equation initial condition $h(z,0)$. The right hand side of (4.20) would be a function of time if the boundary functions of the corresponding PDE were also functions of time. Figure 4.2 plots the solution family for (4.20) sampling various values of $H(0)$ using `Mathematica`. We see indeed as $t \to \infty$ that $H(t) \to 1$. This supports the odd technique of considering $-\mathrm{d}t$ in our derivation. Notice a distinction in the transients for $\gamma < 1$ and $\gamma > 1$. For $\gamma < 1$ we have draining corners and it takes significantly longer to achieve steady state, so much so that for $\gamma = 0$ it is never reached. For the case $\gamma > 1$, filling corners, we see very sharp curvatures which attain steady state rapidly.
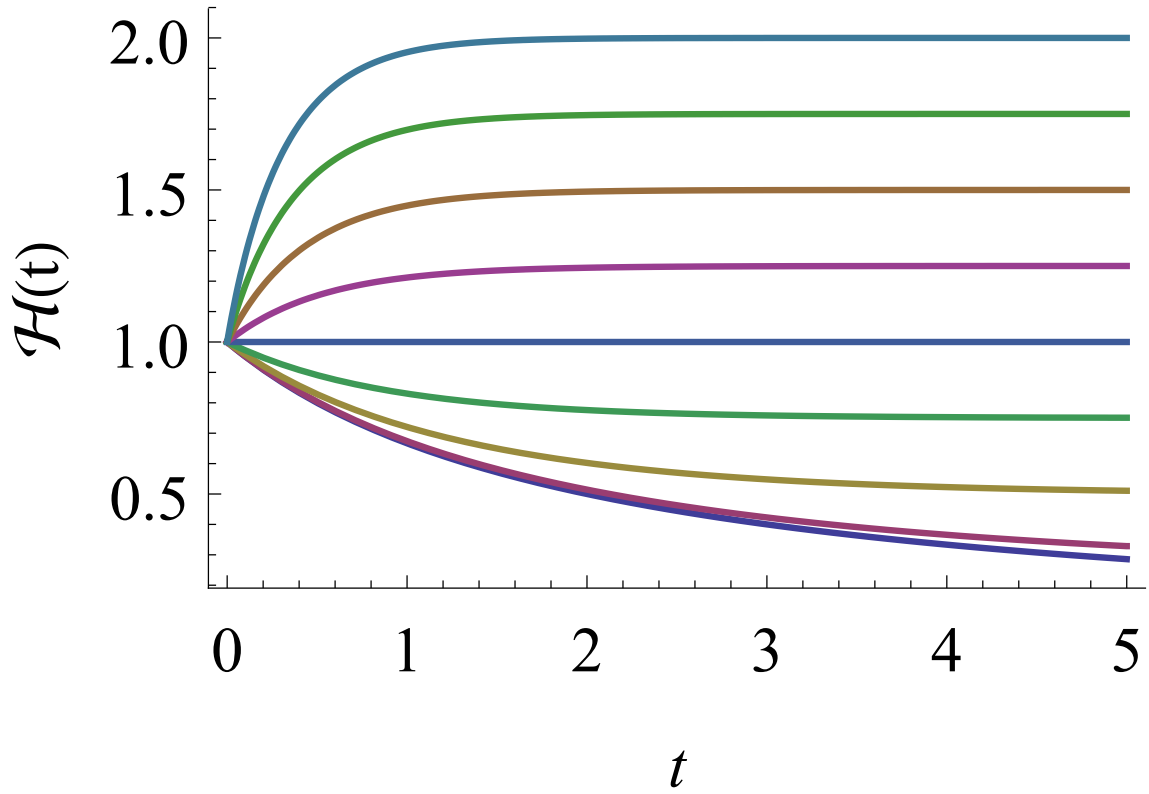
FIGURE 4.2: The solution family is plotted for various initial conditions $\gamma^3 = [0 : 0.25 : 2]$. The solution is starkly different about the point $\gamma = 1$. For initial condition $\gamma > 1$ the solution behaves more more like an exponential. For $\gamma < 1$ the solution is more similar to $H \sim t^{-1}$.

The analytical implicit solution to (4.20) is found to be,

$$3C_0\gamma - 3\frac{\gamma t}{2} = \frac{1}{2}\ln\left[\frac{(H-\gamma)^2}{(H-\gamma)^2 + 3\gamma H}\right] + \sqrt{3}\arctan\left[\frac{2H+\gamma}{\sqrt{3}\gamma}\right]. \tag{4.22}$$

The integration constant C_0 is,

$$\gamma C_0 = \frac{1}{6}\ln\left[\frac{(1-\gamma)^2}{(1-\gamma)^2 + 3\gamma}\right] + \frac{\sqrt{3}}{3}\arctan\left[\frac{2+\gamma}{\gamma\sqrt{3}}\right]. \tag{4.23}$$

This solution comes from various steps of integration by substitution. Analytical inversion to fully determine $H(t)$ is impossible due to the linear combination of transcendental functions.

4.3.1 Asymptotic Analysis for γ

We will now investigate the dynamics for the various magnitudes of γ and t. In each case we get a simplification which can then be inverted, yielding an analytical expression for $H(t)$. There are two branches of this solution defined by γ. For volume draining we are in the domain $\gamma \in (0,1)$, while for volume gaining we investigate $\gamma \in (1,\infty)$. For *each* of these branches we have "early time" large time dynamics $t \to \infty$. These are characterized by $t \to 0$ and $t \to \infty$ respectively. We seek a full picture of the solution $H(t)$ by considering $\gamma \in (0,1)\bigcup(1,\infty)$. Our analysis is all dependent on an initial ansatz of

$$H(t) = \delta_0(\gamma)H_0(t) + \delta_1(\gamma)H_1(t) + \delta_2(\gamma)H_2(t) + \ldots, \tag{4.24}$$

where $\{\delta_i(\gamma)\}$ is an asymptotic sequence such that $\delta_{i+1}/\delta_i \to 0$. We have left the asymptotic sequence general because $\delta_i(\gamma) \equiv \gamma^i$ will not work for the case $\gamma = 1$. It

is certainly of interest to investigate the dynamics about this point for two reasons.

(a) Volume variation in the corner in practice are very small due to creeping flow rates $\beta \approx 1$. Since H represents a root mean square of a meniscus profile the variation in this value due to flow intensity is extremely small. One can show this when considering (2.9) with $0 \leq \beta \leq 1$.

(b) Since we are considering *massively* parallelized corners where $N \sim \mathcal{O}(10^4)$ large jumps in flow rate must come from hundreds of corners becoming blocked instantaneously.

Draining or Filling $\gamma \sim 1$ We are considering variations about so we will say $\gamma^3 = 1 \pm \epsilon$. This will make for a much more cleaner analysis. Cast in this frame work, the asymptotics give us $\mathcal{O}(1)$ and $\mathcal{O}(\epsilon)$ differential systems to solve. The $\mathcal{O}(1)$ system is

$$\frac{dH_0^2}{dt} + H_0^3 = 1, \tag{4.25}$$

$$H_0(0) = 1. \tag{4.26}$$

while the $\mathcal{O}(\epsilon)$ is

$$2\frac{dH_1}{dt} + 3H_1 = \pm 1, \tag{4.27}$$

$$H_1(0) = 0. \tag{4.28}$$

This give an asymptotic solution for volume variation when $\gamma \sim 1$

$$H(t) \sim 1 \pm \frac{\epsilon}{3}(1 - e^{-3t/2}) \tag{4.29}$$

and agrees with the numerical solutions as well. The rest of this chapter could be skipped for this solution has the most useful conclusions. The main one being we can approximate volume gain or drain in a corner exactly like a capacitor in a circuit model. This is because the form of (4.27) is linear and mimics a model of capacitance.

Draining $\gamma \to 0$ For this case the solution is analytical and reveals the $H \sim 1/t$ time scales which come from the original equation.

$$\lim_{\gamma \to 0} H_0(t) = \frac{2}{2 + t}. \tag{4.30}$$

Filling $\gamma > 1$ First when $\gamma \to \infty$, the solution looks like $H(t) = \gamma^3$. A more interesting case though is for large but finite values of $\gamma > 1$. In this case a corner could fill to around two or three times its initial fill level. Situations like this could arise in such a massively large system so we should consider their dynamics. In this case we have no techniques to approximate the solution, this is because we are forces to determine the inversion of (4.22). We can however use our model approximation which we have used previously in sec 3.3 to obtain analytical expressions. We instead solve equation,

$$\eta \frac{dH^3}{dt} + H^3 = \gamma^3 \tag{4.31}$$

73
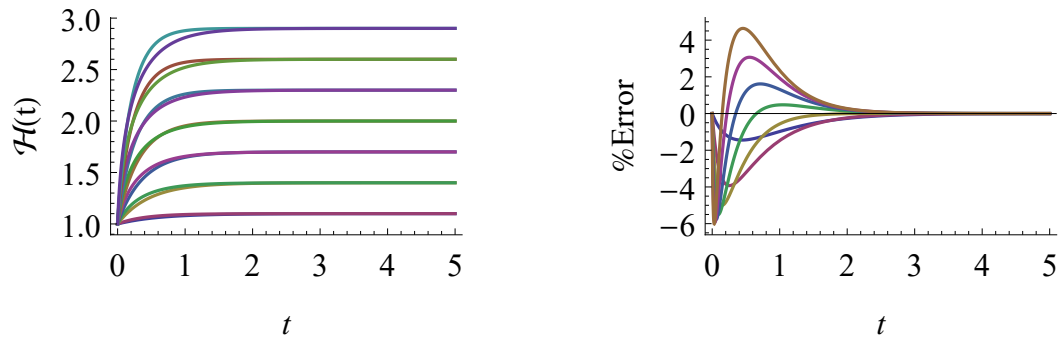
FIGURE 4.3: Model approximation is used to estimate the dynamics of $\gamma \gtrsim 1$. In this plot the parameters are set a $\eta = 0.44$ and plot $\gamma^3 = [0.1 : 0.3 : 3]$. Notice the approximation gets worse as γ increases. This suggests there is some dependence for an *optimal* $\eta(\gamma)$ for a best approximation.

with the same initial condition (4.21). We have inserted an arbitrary scaling term η to compensate for our alteration $H^2 \mapsto H^3$. This equation has the analytical solution

$$H(t) = \left(\gamma^3 + (1 - \gamma^3)e^{-t/\eta}\right)^{1/3}. \tag{4.32}$$

Figure 4.3 is a comparison of these solution for $\gamma^3 \in (1,3)$ and $\eta = 0.44$. The value of η was chosen a heuristic bisection method just as we did in sec 3.3. Determining an *optimal* constant is certainly an interesting question for future research. Figure 4.3.b is the relative error between the solutions. We again find that this model approximation does a fantastic job with a relative error below 4%. In this scenario though there is a caveat. The approximation is getting worse as γ increases. This does suggest there may be some optimal mapping $\eta(\gamma)$ that could prove to provide good approximation for $\gamma \in (1, \infty)$.

74

5 Multiple Corners

In this chapter we only derive the resistances and capacitances of individual circuits. We follow a methodology of a recent micro-fluidic parallel investigations[17]. That is, we lay the foundations for an electrical circuit analogy approximation. The crux of this is to identify a resistance suitable resistance term R_c, and a capacitance C to associate to each corner element. We do some manipulation to derive these quantities, the analytical electrical circuit solution can be found by following the methods of engineering circuit analysis. We do not present such analysis herein as we ran out of time and had to graduate eventually. However we do provide the explicit expressions for R_c, C that could be implemented into a much larger software implementation at a future date.

5.1 Flow Circuit Analogy

We have made an extensive investigation on the dynamics of flow in a corner of finite length. This was all motivate however to answer the question about how a system of several thousand corners would behave. Circuit analogies are quite productive for engineers to make first principles decisions with. Our analysis so far has identified the limits of our 1D model for the corner and now we will continue toward formulating a linear flow circuit. Each corner is modeled as an RC circuit element. In order for liquid to reach these corners as well manifold tubing must installed we will model it

with laminar flow in cylindrical pipes. The relation,

$$\Delta P = \frac{8\mu L}{\pi r^4} Q \tag{5.1}$$

defines a our manifold pressure drops in the system, with flow resistance $R_M = 8\mu L/\pi r^4$. Manifold tubing inherently has many twists curves and bends. Imagine all these effects can be encapsulated in a term $\tilde{R}(i)$ where i will refer to a specific path. This can be modeled with an additional resistance terms such as $R_M(i) = R_M + \tilde{R}(i)$. Corners will be indexed with $i = 1, \ldots, N$. Fig. 5.1 is a schematic depicting this idealization of such a system. Notice that each interior corner is modeled as a parallel unit of a resistor R_c and *capacitor*. This is motivated by the analysis of Sec. 4, where we showed that variations about an average fill level behave linearly.

Circuit Resistance The first question is what is the resistance associated to each corner. We calculate this by considering the dimensional pressure gradient across a steady state corner. We find

$$\Delta P' = \frac{\sigma}{f(\theta, \alpha)} \left(\frac{1}{H_2'} - \frac{1}{H_1'} \right). \tag{5.2}$$

We have already shown that flowrate thru a corner establishes boundary conditions. In general this means $\beta_i = \beta(Q_i)$. The explicit dependence to boundary conditions to be

$$\Delta P = \frac{\sigma}{H_0 f} \left(\sqrt{\frac{3(1 - \beta^5)}{5(1 - \beta^3)}} \right) \left(\frac{1}{\beta} - 1 \right). \tag{5.3}$$

Next we return to the steady state flowrate expression Eq. (2.10), which is as well a function of β and H. We have discussed at length how our model is only valid for
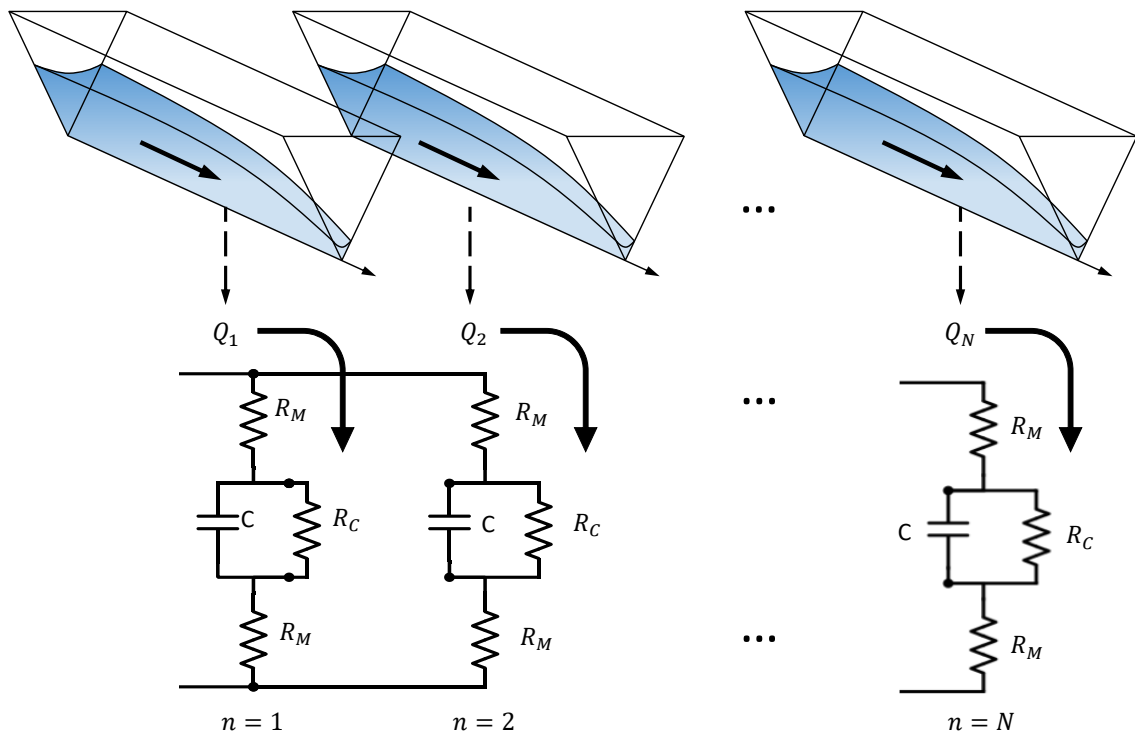
FIGURE 5.1: Massively parallel interior corner idealized as a flow circuit. Importantly there are resistors to and from each corner $R_M(i)$. These manifold resistors are dominant, meaning corners contribute to transients not resistance to a system. A simpler model is then just two resistors attached to a parallel capacitor and wire block.

quasi-steady processes. This motivates an expansion about $\beta = 1$ in Eq. (5.2) and Eq. (2.10), yielding

$$\Delta P' \approx -\frac{(\beta - 1)\sigma}{fH_0}, \tag{5.4}$$

$$Q' \approx \frac{|(\beta - 1)|\sigma H_0^3 \sin^2(\alpha)F_A F_i}{3f\mu L}. \tag{5.5}$$

We equate these expressions by multiplying Eq. (5.5) by $3L\cos\alpha\mu/H_0^4\sin^3$. This gives us an approximate Pousielle type law for the corner resistance,

$$\Delta P' = \frac{3L\mu(1 - \beta)}{H_0^4 \sin^2 \alpha F_A F_i}Q. \tag{5.6}$$

We use well verified approximation $F_i \approx 1/7$ to find the corner resistance to be

$$R_c = \frac{21L\mu(1 - \beta)}{H_0^4 \sin^2 \alpha F_A}. \tag{5.7}$$

We can now investigate a resistance ratio in terms of our old asymptotic parameter ϕ defined in Ch. 3

$$\frac{R_c}{R_M} = \frac{21\phi\pi}{\sin^2 \alpha F_A}\left(\frac{r}{H_0}\right)^4. \tag{5.8}$$

We will remark that yes ϕ is a function of flowrate as seen in Eq. (2.19). However no matter the variation we must lay in the quasi-steady range where flows are at a creeping pace. Given our assumptions this restricts $0 < \phi \ll 1$. The most dominant term however is this ratio of manifold tube radius to the initial corner fill height r/H_0. Considering this ratio it is by necessary design that $r/H_0 < 1$. Since this ratio is then raised to such a large power this resistance ratio is a very small number. Figure 5.2.
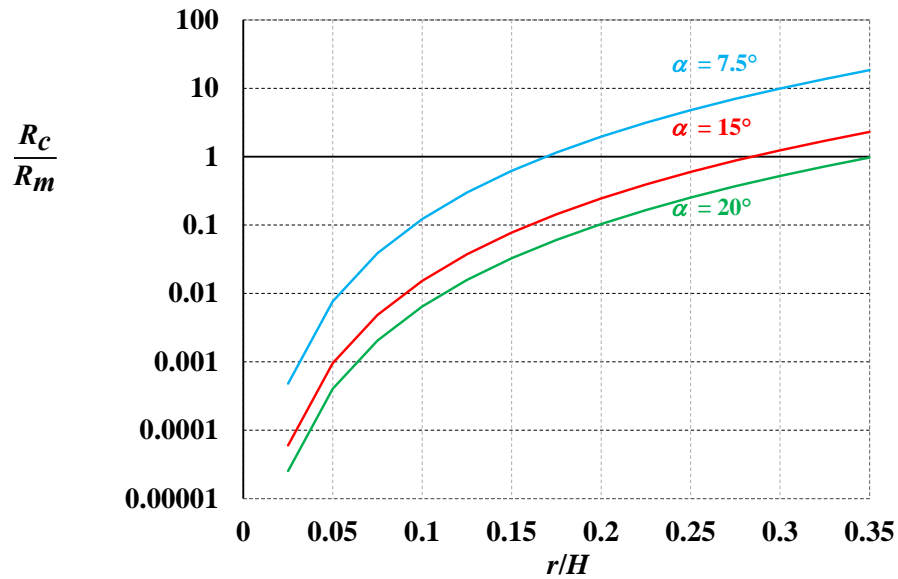
FIGURE 5.2: The ratio of manifold and corner resistance as a function of geometry.

is a plot of this ratio for a sweep of parameters.

Circuit Capacitance We now look for a corner capacitance. This will utilize the first order asymptotic model found in the end of Ch. 4. Recall this expansion we valid for $\gamma = H_\infty/H_0 \approx 1$ and for quasi-steady processes. A capacitance analogy begins with a definition,

$$C\frac{\mathrm{d}m}{\mathrm{d}t} = \frac{\mathrm{d}P}{\mathrm{d}t} \tag{5.9}$$

This definition is borrowed identically from the theory of electricity with a relabeling of variables. We will use the mass of liquid in the corner m instead of electrical charge q and pressure P instead of voltage v for our potential. The capacitance is a proportionality constant between the rate of change of pressure and the rate of change in flowrate. We calculate both side separately then and search for what a

model expression for C would be;

$$\frac{\mathrm{d}m}{\mathrm{d}t} = \rho\frac{\mathrm{d}V}{\mathrm{d}t} = \rho Q$$

$$= \rho\frac{\mathrm{d}}{\mathrm{d}t}\int_0^1 F_A h^2 \mathrm{d}z$$

$$= \rho\frac{\mathrm{d}H_0^2}{\mathrm{d}t}$$

$$\frac{\mathrm{d}P}{\mathrm{d}t} = -\frac{\mathrm{d}}{\mathrm{d}t}\frac{\sigma}{fH_0}$$

$$= \frac{\sigma}{fH_0^2}\frac{\mathrm{d}H_0}{\mathrm{d}t}.$$

We achieve equality if we let

$$C = \frac{\sigma}{2\rho f H_0^3}. \tag{5.10}$$

6 CO_2 Absorption Effects

So far, our governing equation for meniscus height has constant density, viscosity, and surface tension functions. We now make a short analysis on the effects of additional gradients imposed on a corner. The variables of interest are concentration $C(z,t)$ and temperature $T(z,t)$. Their governing partial differential equations are identical. The thermo-physical properties $\{\mu, \rho, \sigma\}$ are functions of both temperature and concentration. A scale analysis shows the dominate effects are in the axial direction with a very slow time scale. The temperature and concentration steady state solutions $T(z), C(z)$, yields model expressions for $\mu(T,C), \sigma(T,C), \mu(T,C)$. These thermo-physical gradients effect the meniscus height when they are substituted into a mass balance across the corner. This derives a new governing equation for the meniscus height along the corner. This new equation is *highly* nonlinear, but importantly all the effects of the property variations is encoded into three coefficient functions $a(z), b(z), c(z)$. This makes a connection between property variation and an analysis of these coefficient functions. More is to be done here as model approximation is still a viable to estimate the full solution of this complex problem. One can compare a numerical solution to an analytical one where the time derivative part of the governing equation is changes with $h^2 \mapsto h^3$, just as was done in sec. 3.3. We do not preform this analysis herein, we only derive the coefficient functions. At a later date which publications will illustrate and quantify just how effective this method is.

6.1 Introduction

The operation for CO2 scrubber necessarily requires an increase in density. An increase in density changes the volume of liquid in the corner which change the resistance and capacitance. We increase the fidelity of the interior corner model by including the effects of sorbent liquid absorbing CO_2 from the ambient air. The process is modeled as a mass flux across the free surface of the liquid. The model produces a new governing equation for the meniscus height that is similar except for an additional terms. These additional term makes an analytical steady state solution intractable. We can however identify the functional connection between property variations and coefficient functions $a(z), b(z), c(z)$. The effects of these coefficient functions slightly alter the meniscus height.

The degassing phase of a CO_2 scrubber introduces heat to boil off the absorbed gas. The addition of a temperature gradient alters the surface tension, viscosity, and density properties of the liquid. Changes in these properties directly contribute to the characteristic time expression. The goal of this analysis is to calculate correction factors for the degassing and absorbing operations. We will assume that the contact angle θ remains constant. From experiments we know this not to be the case. Slight molecular changes to a fluid can result in reasonably large hysteresis $\Delta\theta \sim 10°$. The analysis of constant θ only show how insignificant the effects are to meniscus height $h(z,t)$. These functions $\sigma(T)$ and $\mu(T)$ are left arbitrary for now but be addressed later on. We derive a new governing equation for meniscus height $h(z,t)$ and find new terms. An entire class of steady state solutions is possible that are dependent on $\sigma(T)$, $\mu(T)$, and $\rho(T)$.

6.2 Mathematical Formulation

Critical dimensions are noted for the slender finite interior corner capillary flow sketched in Fig. 1.5. The corner is partially-filled with a wetting liquid of viscosity μ and surface tension σ and satisfies the Concus Finn condition. The function $h(z,t)$ is the height of the meniscus center-line along the corner, where $h(0,t) \equiv H_1$ is the inlet boundary height, used also as the characteristic height of the flow, L is the corner length, and $h(L,t) \equiv H_2 > 0$. A variety of similarity solutions arise [3, 28, 4] for the condition $h(L,t) = 0$. The slenderness ratio $\epsilon = H_1/L$ appears in the dimensionless momentum equations [9] and serves as a small parameter allowing asymptotic analyses when $\epsilon^2 \ll 1$. This limit enables the lubrication approximation in the momentum balance while reducing the normal stress condition at the free surface to the Young-Laplace equation, which is solved analytically to find the entire transient free surface as a series of circular arcs in x-y planes. This result allows us to define a dimensional local radius of curvature $R(z,t) = fh(z,t)$ for any point $z_0 \in [0,L]$, where

$$f(\alpha,\theta) = \frac{\sin\alpha}{\cos\theta - \sin\alpha} \tag{6.1}$$

is a geometric surface curvature function. We note that the axial pressure is given by $P = \sigma/R$.

Nondimensionalization of the governing equations is established using the scales listed in Table 6.1 The dimensionless momentum, concentration, and heat equations adopt the material derivative operator $\mathrm{D}/\mathrm{D}t \equiv \partial/\partial t + (\mathbf{V}\cdot\nabla)$. The critical dimensionless groups that arise are Suratman number $\mathsf{Su} = \rho_0\sigma_0 L/\mu_0^2$, species Peclet number $Pe_D = \sigma_0 L/\mu_0 D$, and thermal Peclet number $Pe_\kappa = \sigma_0 L/\mu_0 \kappa$ (or thermal Marangoni

number), where D and κ are the liquid species and thermal diffusivities, respectively. These groups are essentially Reynolds and Peclet numbers defined on the capillary velocity scale σ_0/μ_0. The superscript $^+$ adds geometric scaling to $\mathsf{Su}^+ = \mathsf{Su}\sin^4\alpha/f$, $Pe_D^+ = Pe_D\sin^4\alpha/f$, and $Pe_\kappa^+ = Pe_\kappa\sin^4\alpha/f$. We will also define a dimensionless Laplacian operator

$$\nabla^2 \equiv \sin^2\alpha\frac{\partial^2}{\partial x^2} + \cos^2\alpha\frac{\partial^2}{\partial y^2} + \epsilon^2\sin^2\alpha\frac{\partial^2}{\partial z^2}. \tag{6.2}$$

With these definitions the general system of equations is

$$\epsilon^4\mathsf{Su}^+\frac{\mathrm{D}u}{\mathrm{D}t} = -\frac{\partial p}{\partial x} + \epsilon^2\mu\nabla^2 u, \tag{6.3}$$

$$\epsilon^4\tan^2\alpha\,\mathsf{Su}^+\frac{\mathrm{D}v}{\mathrm{D}t} = -\frac{\partial p}{\partial y} + \epsilon^2\tan^2\alpha\mu\nabla^2 v, \tag{6.4}$$

$$\epsilon^2\mathsf{Su}^+\frac{\mathrm{D}w}{\mathrm{D}t} = -\frac{\partial p}{\partial z} + \mu\nabla^2 w, \tag{6.5}$$

$$\frac{\partial\rho A}{\partial t} + \frac{\partial\rho Q}{\partial z} = 0, \tag{6.6}$$

$$\epsilon^2 Pe_D^+\frac{\mathrm{D}C}{\mathrm{D}t} = \nabla^2 C, \tag{6.7}$$

$$\epsilon^2 Pe_\kappa^+\frac{\mathrm{D}T}{\mathrm{D}t} = \nabla^2 T. \tag{6.8}$$

The associated boundary conditions in terms of the velocity vector field $\mathbf{V} = [u, v, w]^T$, and the *stress tensor* $\mathbf{T} = \mu(\nabla\mathbf{V} + \nabla\mathbf{V}^T) - P\mathbf{I}$ are

$$\mathbf{n}\cdot\mathbf{T}\mathbf{n} = \sigma(\nabla\cdot\mathbf{n}), \tag{6.9}$$

$$\mathbf{n}\cdot\mathbf{T}\mathbf{t} = \nabla\sigma\cdot\mathbf{t}. \tag{6.10}$$

Thermal gradients cause $\nabla\sigma \neq 0$ which induce additional surface stresses. Inertial

84

TABLE 6.1: A summary of all dimensionless variables. The scaling is motivated by the geometry shown in fig. 1.5. Dimensional quantities are indicated with an uppercase prime.

Length	Velocity	Properties	Other
$x = x'/H_1$	$u = u'/\epsilon W_0$	$\sigma = \sigma'/\sigma_0$	$P = H_1 f P'/\sigma_0$
$y = y'/H \tan \alpha$	$v = v'/\epsilon W_0 \tan \alpha$	$\rho = \rho'/\rho_0$	$t = W_0 t'/L$
$z = z'/L$	$w = w'/W_0$	$\mu = \mu'/\mu_0$	$A = A'/H_1^2 \tan \alpha$
$h = h'/H_1$	$W_0 = \epsilon \sigma_0 \sin^2 \alpha / f \mu_0$		$\epsilon = H_1/L$
	$\langle w \rangle = \langle w \rangle'/W_0$		$T = T'/T_0$
	$Q = Q'/W_0 H_1^2 \tan \alpha$		$C = C'/C_\infty$

terms may be neglected at zeroth order when $\epsilon^2 \mathsf{Su}^+ \ll 1$, $\epsilon^2 Pe_D^+ \ll 1$, and $\epsilon^2 Pe_\kappa^+ \ll 1$, which is frequently the case due to the slenderness of the flow.

Concentration Gradients

The presence of concentration gradients at the interface create variations in fluid thermophysical parameters ρ, σ, μ. Surface tension varies with temperature and concentration and can create additional shear flows at the interface. Viscosity variations alter the shear stresses at the wall causing an increase or decrease of flow magnitude. Finally density variations due to gas absorption alter the inertial character of the flow. In the limit of $\epsilon^2 Pe_D^+ \to 0$, eq. (6.7) reduces to a Laplace equation for $C(x, y, z)$. Due to the scaling in eq. (6.2), zeroth order effects are in the x, y cross dimensional plane, while first order effects of ϵ^2 are in the axial z direction. In second order effects of order ϵ^4, concentration has variations in the x-y plane. These effects model the concentration *distribution* in the thin penetration layer on near the interface. Second order effects will be ignored herein. Since the zeroth order effects only imply that concentrations must be constant in a cross sectional plane, we will refer to the concentration field as C and not C_1 as would be the case in standard asymptotic analysis,

85

These effects are governed by

$$\frac{\partial C}{\partial t} = \frac{\sin^2 \alpha}{Pe_D^+} \frac{\partial^2 C}{\partial z^2}, \tag{6.11}$$

$$C(0,t) = 0 \quad \& \quad C(1,t) = 1, \tag{6.12}$$

$$C(z,0) = 1. \tag{6.13}$$

The boundary conditions and initial conditions require some discussion. Our boundary conditions model pure liquid entering the corner on the left hand side at $z = 0$ and fully saturated liquid at the outlet, $z = 1$. We impose an initial condition that at the beginning of this process our corner is fully saturated at C_∞. These conditions then model the transients and behavior of pure liquid continually refilling a corner which is a process common in CO_2 scrubbing application [12, 11]

Temperature Gradients

Temperature gradients follow an identical formulation as concentration. The zeroth order effects conclude constant temperature values in an arbitrary cross section within the corner. The first order effects of ϵ^2 imply linear axial variations in the z-direction. We again will neglect the second order effects since they are on the order of ϵ^4, and further more refer to The first order system of equation is found to be

$$\frac{\partial T}{\partial t} = \frac{\sin^2 \alpha}{Pe_\kappa^+} \frac{\partial^2 T}{\partial z^2}, \tag{6.14}$$

$$T(0,t) = 1 \quad \& \quad T(1,t) = T_{out}, \tag{6.15}$$

$$T(z,0) = T_{out}. \tag{6.16}$$

Pressure Gradients

We consider the zeroth order effects of in the limit of $\epsilon^2 \mathsf{Su}^+ \to 0$. In the slender flow limit, $\epsilon^2 \ll 1$ and $\epsilon^2 f \ll 1$, the momentum eqs. (6.3)-(6.5) and eqs. (6.18), (6.19) reduce to,

$$\frac{\partial p}{\partial z} = \mu \left(\sin^2 \alpha \frac{\partial^2 w}{\partial y^2} + \cos^2 \alpha \frac{\partial^2 w}{\partial x^2} \right), \tag{6.17}$$

$$0 = w(x, y = \pm x), \tag{6.18}$$

$$\frac{f}{\sin \alpha} \frac{\mathrm{d}\sigma}{\mathrm{d}z} = \mu \left(K_1(\alpha) \frac{\partial w}{\partial x} - K_2(\alpha) \frac{\partial w}{\partial y} \right). \tag{6.19}$$

We have defined geometrical scaling functions $K_1 = \sin^2 \alpha / (\sin^2 \alpha + (S')^2 \cos^2 \alpha)^{1/2}$ and $K_2 = S' \cos^2 \alpha / (\sin^2 \alpha + (S')^2 \cos^2 \alpha)^{1/2}$, where $S(y) = x$ defines the interface curve at each cross-sectional plane illustrated in fig. 1.6.

There are two critical facts about this system of equations. First the system is known to have a unique solution $w(x, y)$ which allows us to define an average velocity as

$$\langle w \rangle = \frac{1}{A} \int_{A(z,t)} w(x, y) \mathrm{d}A. \tag{6.20}$$

Second the system is *linear* which allows us to construct the solution via superposition or two solutions. The first solution $w_p(x, y)$ is the pressure driven part where we let $\mathrm{d}\sigma/\mathrm{d}z = 0$ in eq. (6.19). The second is the shear driven solution $w_s(x, y)$ where $\partial p/\partial z = 0$ in eq. (6.17). The solution is a linear *functional* combination of these two functions given by,

$$w(x, y) = \frac{1}{\mu} \frac{\partial p}{\partial z} w_p(x, y) + \frac{f}{\mu \sin \alpha} \frac{\mathrm{d}\sigma}{\mathrm{d}z} w_s(x, y) \tag{6.21}$$

87

We substitute eq. (6.21) into eq. (6.20) and abstract the details of the integration over the cross-sectional area into $\mathcal{O}(1)$ geometrical functions F_i, E_i. These functions have been found to be weakly dependent on α and sufficient approximations is made with $1/7 \lesssim F_i \lesssim 1/8$. We will assume the same can be said for E_i. Moreover, because of eq.(6.11), (6.14) we know that temperature and concentration variation is predominantly in the z-direction. This justifies that the coefficient functions that appear in eq.(6.21) play no role in the integration. We note that $P = -\sigma(z)/fh(z,t)$ which leads us to an expression for average axial velocity,

$$\langle w \rangle = -\frac{F_i}{\mu}\left(\sigma\frac{\partial h}{\partial z} - \frac{1}{h}\frac{\mathrm{d}\sigma}{\mathrm{d}z}\right) + \frac{E_i}{\mu}\frac{fh}{\sin\alpha}\frac{\mathrm{d}\sigma}{\mathrm{d}z} \tag{6.22}$$

Continuity

Our final governing dynamical equation comes from the integrated continuity equation eq. (6.6). Substituting $Q = \langle w \rangle A$, $A = F_A(\alpha, \theta)h^2$, and eq. (6.22) into eq. (6.6) and defining $E = 1 + E_i f/F_i \sin\alpha$ we derive

$$\frac{\partial h^2}{\partial t} = a(z)\frac{\partial^2 h^3}{\partial z^2} + b(z)\frac{\partial h^3}{\partial z} + c(z)h^3, \tag{6.23}$$

$$h(0,1) = 1 \quad \& \quad h(1,t) = \frac{H_2}{H_1} \equiv \beta \tag{6.24}$$

$$h(z,0) = g(z), \tag{6.25}$$

where have defined

$$a(z) = \frac{F_i \sigma}{3\mu} \tag{6.26}$$

$$b(z) = \frac{F_i}{3\rho} \left\{ \frac{\mathrm{d}}{\mathrm{d}z} \left(\frac{\rho \sigma}{\mu} \right) - 3E \frac{\rho}{\mu} \frac{\mathrm{d}\sigma}{\mathrm{d}z} \right\} \tag{6.27}$$

$$c(z) = -\frac{F_i E}{\rho} \left\{ \frac{\mathrm{d}}{\mathrm{d}z} \left(\frac{\rho}{\mu} \right) \frac{\mathrm{d}\sigma}{\mathrm{d}z} + \left(\frac{\rho}{\mu} \right) \frac{\mathrm{d}^2\sigma}{\mathrm{d}z^2} \right\}. \tag{6.28}$$

Here we have defined $E = 1 + fE_i/F_i \sin \alpha$. We have set the corner to have some initial meniscus height curve $g(z)$ at $t = 0$. Our boundary conditions imply a constant pressure gradient across the corner. The majority of the analysis herein focuses on the effects of the magnitudes and functional forms of equations (6.26), (6.27), (6.28). Notice that by selecting equations of state such that $\sigma(T, C), \rho(T, C), \mu(T, C)$ coupled with the steady state solutions to eq. (6.11) and eq. (6.14) make (6.23) a fully defined differential system. This makes the study of thermophysical parameter variation in a slender corner an analysis of defining equation of states. Currently there is no theory to derive these equations of state for a liquid which forces us to empirical formulae obtained from experiments or linear approximations. The later case is suitable if we consider only small temperature and concentration gradients.

7 The Pinned Corner

Another layer of complexity for the interior corner flow dynamics is the case of a pinned contact line. This occurs when the fluid has filled the corner completely. When the fluid pins to the corner the contact line can freely increase or decrease creating two cases. One is if it increases to the liquid's contact angle on the exterior top surface and wet outward. The other is if it decrease until it equals the contact angle on the interior of the corner, de-pin, and leave us with the results of this thesis. This variable angle creates a non-constant area scale function F_A which can no longer be taken out of the spatial derivative in the governing equation. However, the meniscus height in this case is only a function of the contact line angle $h(\theta(z,t))$. We can formulate a new governing differential equation using the chain rule and the geometrical functions $F_A(\theta)$, $h(\theta)$, and $f(\theta)$. This analysis gives a path for future work to create much more accurate models of the corner flows which, in operation, are usually pinned. Even if not pinned, sensitivity derivative show the largest contribution to meniscus height is contact angle hysteresis. As the liquid properties change over large time intervals the contact angle will indeed change. This long scale dynamic will be of great importance to the future of understanding this passive system.

7.1 Fully filled corners

Describe fully filled corners and the problems they arise in. Almost always in practice corners end up fully filled and with the liquid pinned at the top corner. We seek to have corners as full as possible, since larger heights correspond to more surface area for diffusion to take place. Previous analysis focuses on the depinned problem because of the soluble problems it provides. This last section aims to set the stage for new investigations which are more realistic for engineering designs. We will keep all of the assumptions made in chapter 1 but relax the condition on $F_A = F_A(\theta, \alpha)$. We also must assume that the corner geometry is constant in the axial direction $\alpha \neq \alpha(z)$. There is still much further work to be done in estimation of more complex cases. The most interesting case would be a combination of both pinned and depinned dynamics occurring within the corner. This would occur if the upstream pressure is low enough. The location where the fluid depins would be some $z_0 \in (0, L)$. At this point the meniscus will form a cusp and be non-differentiable. This makes hope of an equation to describe both sections impossible. A patching between both solutions would be necessary.

7.2 Mathematical Formulation

For the pinned condition we shall reformulate our governing equation only slightly. We will shift our focus to $\theta(z, t)$. The geometry illustrated in figure 7.1 shows $h = \mathcal{H} - s$. The circle arc height s is a trigonometric formula.

$$h = \mathcal{H}(1 + f(1 - \cos \delta))^{-1}. \tag{7.1}$$
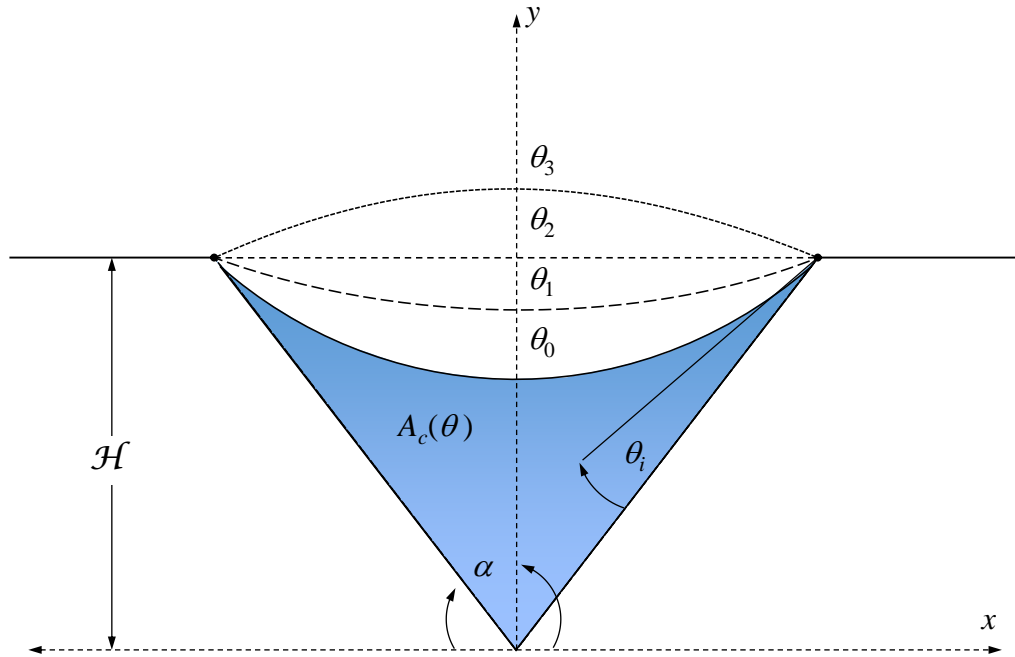
FIGURE 7.1: Each subscript refers to an advancing time step. Here the contact angle begins at θ_0 and the next time step is at θ_1. The cross sectional area is now a function of this changing contact line angle. The height of the meniscus changes one-to-one with this contact line angle.
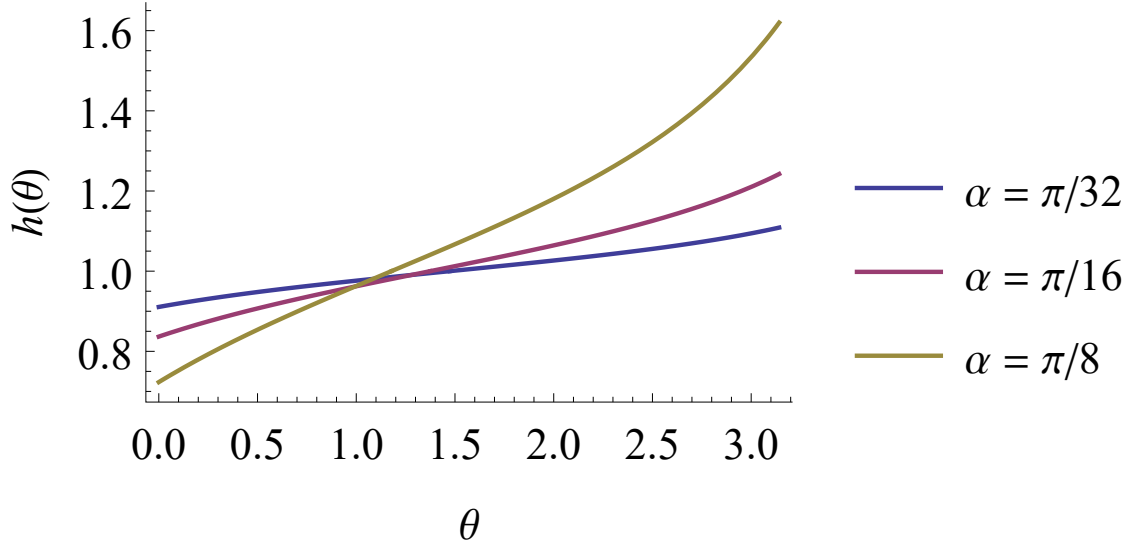
FIGURE 7.2: Here we have set $\mathcal{H} = 1$. As $\theta(z,t)$ varies we see $h(\theta)$ is monotonically increasing function for all values of α. For smaller values of α i.e. thin corners, we see less variation in height due to θ.

As long as one knows the height of the interior corner while empty the meniscus height can be calculated. Recall that $\delta = \pi/2 - (\alpha + \theta)$ and is simply a shifting of angles. Any derivatives simply make a change of sign as the angles are inversely proportional. We plot the function for various half interior angles in figure 7.2. All pinned dynamics correspond to sliding along these curves for a given α. Our goal is to determine the suitable θ parameterization along these curves.

What is important about eq. (7.1) is that we have set up the composition $h(\theta)$. So area can be thought of as

$A(z,t) = F_A(\theta(z,t))h^2(\theta(z,t))$ and $Q(z,t) = F_i A(\theta(z,t))\partial_z h(\theta(z,t))$ These functional form are far to nonlinear to make any analysis useful. We shall in-stead state that $A = A(\theta)$ and use eq (7.1) for our governing equation. The governing

equation comes from the same mass balance made in chapter 1.

$$\frac{\partial A}{\partial t} = -\frac{\partial Q}{\partial z},$$

$$\frac{\partial A}{\partial \theta}\frac{\partial \theta}{\partial t} = -F_i \frac{\partial}{\partial z}(A\frac{\partial h}{\partial \theta}\frac{\partial \theta}{\partial z}).$$

It is helpful now to denote $\frac{dA}{d\theta} = A'$ and to shift to subscript partial differentiation. We carry on and find,

$$A'\theta_t = F_i A' h_\theta \theta_z^2 + F_i A(h_{\theta\theta}\theta_z^2 + h_\theta\theta_{zz}), \tag{7.2}$$

$$\theta_t = (F_i h_\theta + F_i \frac{A}{A'}h_{\theta\theta})\theta_z^2 + (F_i \frac{A}{A'}h_\theta)\theta_{zz}, \tag{7.3}$$

$$\theta_t = a(\theta)\theta_z^2 + b(\theta)\theta_{zz}. \tag{7.4}$$

In (7.4) we have abstracted the coefficient functions to $a(\theta)$ and $b(\theta)$. The properties of these function is the majority of the rest of this analysis. One should notice the remarkable similarity to the previous governing equation for the meniscus height. But at this stage, one could solve this equation and use the solution for $\theta(z,t)$ to calculate meniscus height, flowrate, and surface area, $\{h, Q, S_A\}$.

7.3 Analysis of $a(\theta)$ and $b(\theta)$

The full expressions for these coefficient functions are quite formidable. The simplest analysis we can preform is to plot both functions for small domains of θ. Figure 7.3 and 7.4 are plots of both $a(\theta)$ and $b(\theta)$. Whatever the output of the function $\theta(z,t)$ is, the value of $a(\theta(z,t)), b(\theta(z,t))$ must exist on these curves. We plot the entire domain of contact angles as well. The right of the center red line are non-wetting

94

liquids, to the left are the wetting liquids. We select three values of of the half interior corner $\alpha = \{7.5°, 15°, 25°\}$. These angles represent thin, medium, and wide corners respectively. Figure xxa. shows that the entire output of $a(\theta) < 2, \forall \theta \in (0, \pi)$. Figure xxb shows similarly that $0 < b(\theta) < \theta, \forall \in (\theta_{min}, \pi)$, where $\theta_{min} \approx 0.6$ radians. There is a major conclusion just from this.

The depinned case can be thought of as just a relabeling of variables $\theta \mapsto h$, with specific coefficient functions $a(h) \equiv 2$ and $b(h) \equiv h$

$$\theta_t = a(\theta)(\theta_z)^2 + b(\theta)\theta_{zz}$$

$$h_t = 2(h_z)^2 + hh_{zz}.$$

From the above discussion we can conclude now that

$$\theta_t < h_t. \tag{7.5}$$

This is quite a stunning result. We know that the dynamics of a pinned corner now are much slower than corners with free contact lines. There is also another major difference between the structure of the these equations. This is that $a(\theta) < 0$ for some values of θ depending on the corner angle.

7.4   Approximate Solution

A solution for (7.4) is not available. The form of the equation may be simpler, but the shear nonlinearity and number of terms in the coefficient functions $a(\theta)$ and $b(\theta)$ make even the modest asymptotic analysis quite ugly. At this point we simply change the governing equation to yield a solution. What is incredible about this one is all we

95
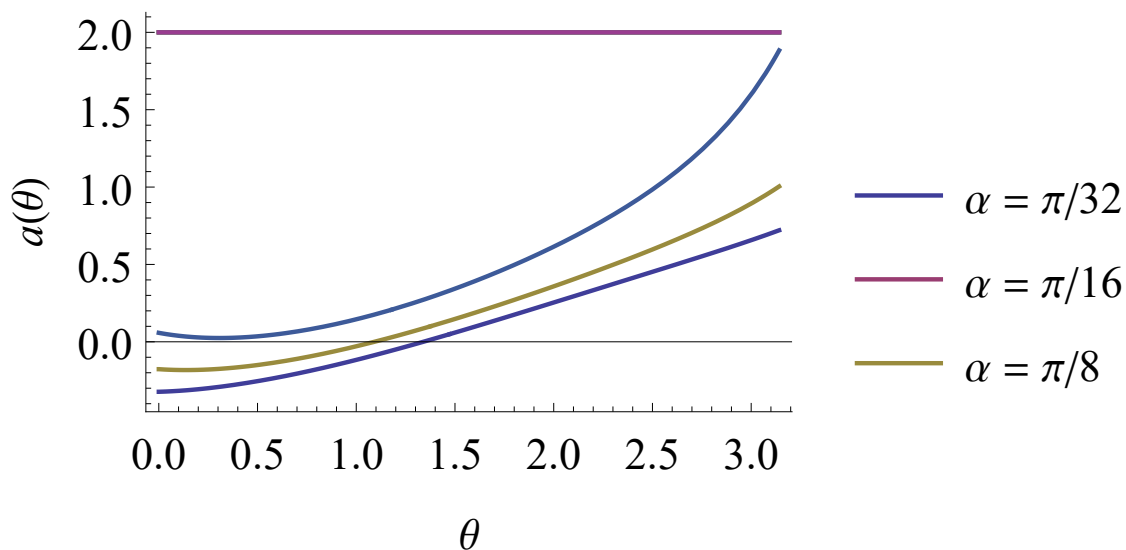
FIGURE 7.3: A plot of coefficient function $a(\theta)$. The thick line above indicates that $a(\theta) < 2$. The thin black line is the zero line. Notice that $a(z)$ may take on positive or negative values
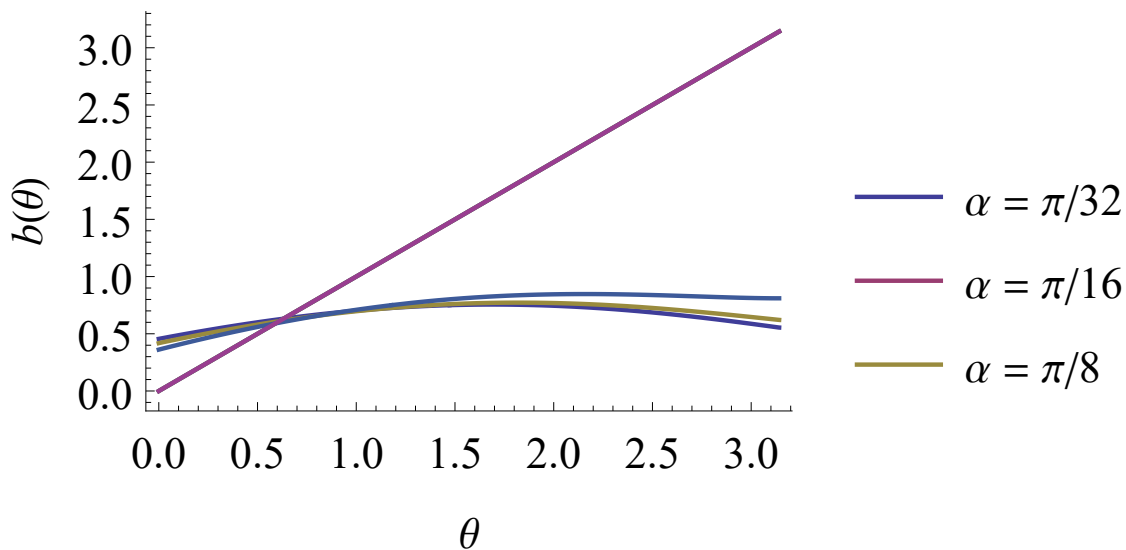
FIGURE 7.4: A plot of coefficient function $b(\theta)$. The thick line shows that $b(\theta) < \theta$, as long as $\theta \gtrsim 0.5$. Notice that comparing to Fig. 7.3, $b(\theta)$ has a much weaker dependence to α. Also, unlike $a(\theta)$, $b(\theta)$ is a strictly positive function.

have to do is replace $b(\theta) \mapsto \langle b \rangle$. This makes the differential equation to solve instead

$$\theta_t = \langle b \rangle \theta_{zz}, \tag{7.6}$$

with boundary conditions $\theta(0,t) = \theta_1$, $\theta(1,t) = \theta_2$ and initial condition $\theta(z,0) = \theta_0$. The motivations to do this come only from how successful this method has been thru out this entire thesis. Figure 7.5, 7.8 compares the solutions to these two differential equations. We have three solutions compared. There is the numerical solution to the original equation, the numerical solution to the approximation equation, and the infinite series analytical solution to approximation model. The solutions are nearly coincident. Surprisingly the standard linear heat equation does a better job at approximating the pinned case. We observe that the largest error in this approximation is at the beginning when adjusting from an initial condition. An immediate gap that could be filled is to mimic the work of [42], and prove that the pinned governing equation is also Lyapunov stable, or better yet asymptotically or exponentially stable. I myself cannot add any more to this analysis but encourage other to take a stab at it, the analysis is quite painful given the shear size of the coefficient functions $a(\theta), b(\theta)$.

With that I will end encouraging you, the reader, to maybe consider model approximation when facing on nonlinear diffusion in finite domains. I will end with a most surprising fact that even in a dynamical boundary function case just we studied in sec. 3.3, eq. 7.6 does a fantastic job. We illustrate this finally with fig. 7.7 and fig. 7.8. This error still was bounded just as it was in sec. 3.3 never becoming greater than 10% relative error. Fascinating.
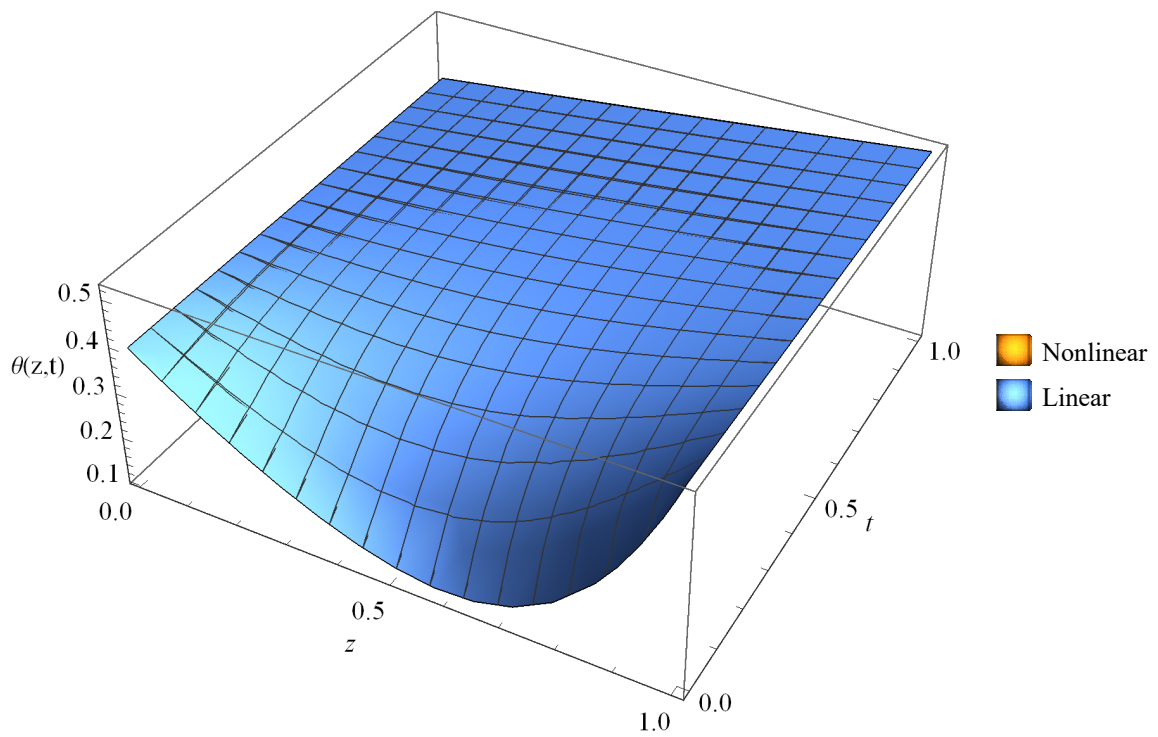
FIGURE 7.5: An example of the two solution surfaces superimposed on one another. The approximation is so good that the two surface are coincident making the entire surface look blue. This example is done with $\alpha = \pi/8, \theta_1 = \pi/6, \theta_2 = \pi/8, \theta(z,0) = \theta_2 z^2 + \theta_1(z-1)^2$
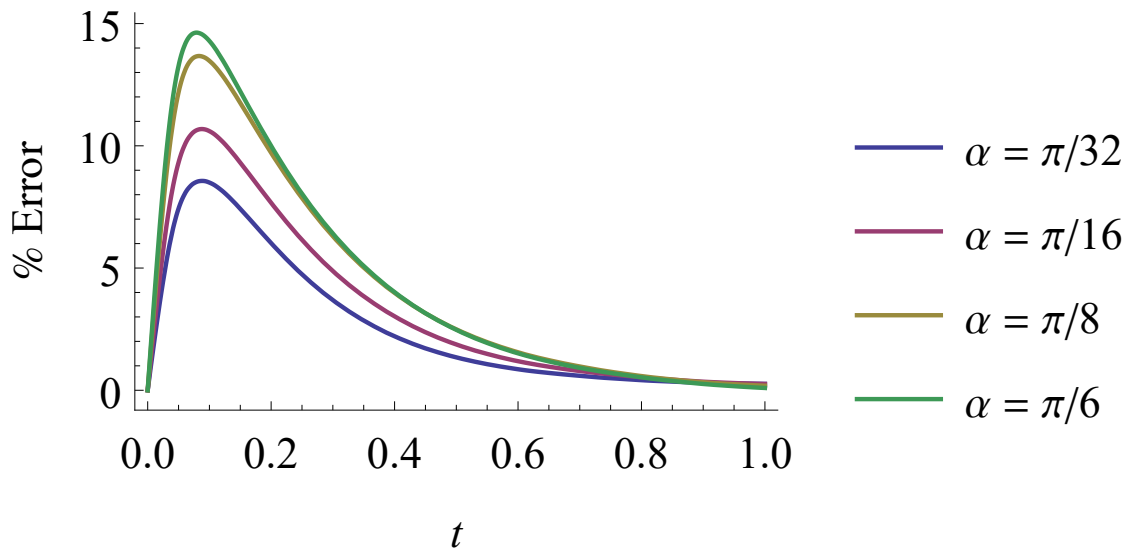
FIGURE 7.6: We plot the relative error between surfaces along the $z = 0.5$ plane, where the error is largest since it is the furthest from the boundaries. The initial condition is kept the same as it is in Fig. 7.5, The relative error of this approximation is inversely proportional to α. The error however decays do to a 1% at steady state.
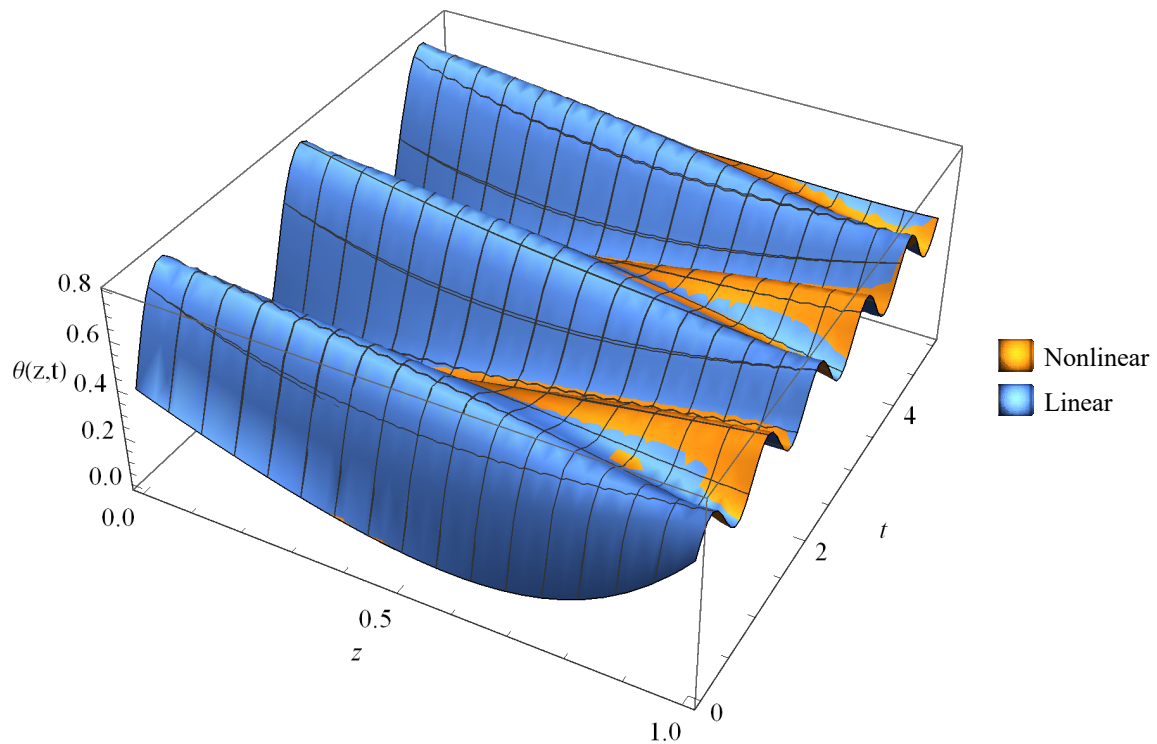
FIGURE 7.7: A model comparison for time dependent boundary conditions. The boundary conditions here are $\theta(0, t) = \frac{\pi}{8} + 0.4 \sin(\pi t)$, $\theta(1, t) = \frac{\pi}{6} + 0.1 \sin(2\pi t)$.
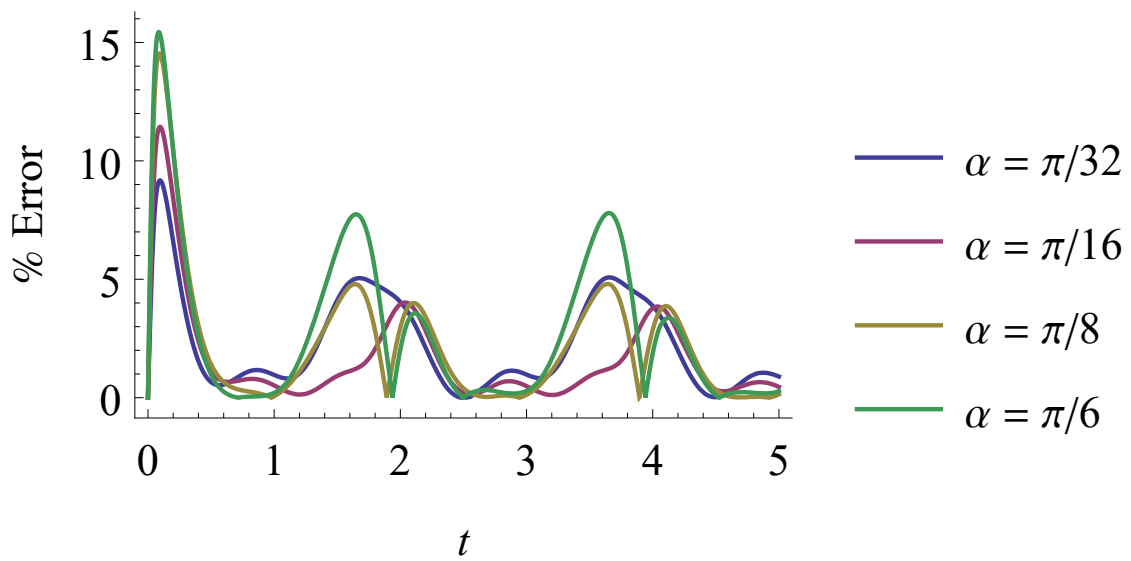
FIGURE 7.8: We plot the relative error in the same fashion as we did in Fig. 7.6. The relative error of this approximation is still inversely proportional to α, now there is no decay to a steady state. However, the error never exceeds 10% as time continues.

Bibliography

[1] P. Concus and R. Finn, "On the behavior of a capillary surface in a wedge," *Proceedings of the National Academy of Sciences of the United States of America*, vol. 63, no. 2, p. 292, 1969.

[2] M. M. Weislogel, "Compound capillary rise," *Journal of Fluid Mechanics*, vol. 709, pp. 622–647, 2012.

[3] M. M. Weislogel, J. A. Baker, and R. M. Jenson, "Quasi-steady capillarity-driven flows in slender containers with interior edges," *Journal of fluid mechanics*, 2011.

[4] M. M. Weislogel and J. T. McCraney, "The symmetric draining of capillary liquids from containers with interior corners," *Journal of Fluid Mechanics*, vol. 859, p. 902–920, 2019.

[5] L. Romero and F. Yost, "Flow in an open channel capillary," *Journal of Fluid Mechanics*, vol. 322, pp. 109–129, 1996.

[6] M. Dong and I. Chatzis, "The imbibition and flow of a wetting liquid along the corners of a square capillary tube," *Journal of colloid and interface science*, vol. 172, no. 2, pp. 278–288, 1995.

[7] A. Myshkis, V. Babskii, N. Kopachevskii, L. Slobozhanin, A. Tyuptsov, and R. Wadhwa, "Low-gravity fluid mechanics," *Translated from the Russian by Wadhwa*, p. 584, 1987.

[8] D. Langbein, "Fluid statics and dynamics in microgravity," *Journal of Physics: Condensed Matter*, vol. 2, pp. 491–498, Dec. 1990.

[9] M. M. Weislogel and S. Lichter, "Capillary flow in an interior corner," *Journal of Fluid Mechanics*, vol. 373, p. 349–378, 1998.

[10] A. Ponomarenko, D. Quéré, and C. Clanet, "A universal law for capillary rise in corners," *Journal of Fluid Mechanics*, 2011.

[11] D. ElSherif and J. Knox, "International space station carbon dioxide removal assembly (iss cdra) concepts and advancements," *Ices 2005*, 08 2005.

[12] R. Carey, A. Gomezplata, and A. Sarich, "An overview into submarine co2 scrubber development," *Ocean Engineering*, vol. 10, no. 4, pp. 227–233, 1983.

[13] D. Langbein, R. Grossbach, and W. Heide, "Parabolic flight experiments on fluid surfaces and wetting," *ApMT*, pp. 198–211, 1990.

[14] R. M. Jenson, A. P. Wollman, M. M. Weislogel, L. Sharp, R. Green, P. J. Canfield, J. Klatte, and M. E. Dreyer, "Passive phase separation of microgravity bubbly flows using conduit geometry," *International journal of multiphase flow*, vol. 65, pp. 68–81, 2014.

[15] J. McCraney, M. M. Weislogel, and P. Steen, "Openfoam simulations of late stage container draining in microgravity," *Fluids*, vol. 5, no. 4, p. 207, 2020.

[16] G. B. Abadi and M. Bahrami, "A general form of capillary rise equation in micro-grooves," *Scientific reports*, vol. 10, no. 1, pp. 1–11, 2020.

[17] S. N. Calver, E. A. Gaffney, E. J. Walsh, W. M. Durham, and J. M. Oliver, "On the thin-film asymptotics of surface tension driven microfluidics," *Journal of Fluid Mechanics*, vol. 901, p. A6, 2020.

[18] R. Finn, *Equilibrium capillary surfaces*, vol. 284. Springer Science & Business Media, 2012.

[19] E. W. Washburn, "The dynamics of capillary flow," *Phys. Rev.*, vol. 17, pp. 273–283, Mar. 1921.

[20] R. Bressler and P. Wyatt, "Surface wetting through capillary grooves," *Journal of Heat Transfer*, vol. 92, 1970.

[21] P. Ayyaswamy, I. Catton, and D. Edwards, "Capillary flow in triangular grooves," *Journal of Fluid Mechanics*, 1974.

[22] R. Lenormand, C. Zarcone, *et al.*, "Role of roughness and edges during imbibition in square capillaries," in *SPE annual technical conference and exhibition*, Society of Petroleum Engineers, 1984.

[23] T. Ransohoff and C. Radke, "Laminar flow of a wetting liquid along the corners of a predominantly gas-occupied noncircular pore," *Journal of Colloid and Interface Science*, vol. 121, no. 2, pp. 392–401, 1988.

[24] D. Langbein, "The shape and stability of liquid menisci at solid edges," *Journal of Fluid Mechanics*, vol. 213, pp. 251—-265, 1990.

[25] M. Dreyer, A. Delgado, and H.-J. Path, "Capillary rise of liquid between parallel plates under microgravity," *Journal of Colloid and interface science*, vol. 163, no. 1, pp. 158–168, 1994.

[26] M. M. Weislogel and S. H. Lichter, "A spreading drop in an interior corner: theory and experiment," *Microgravity Science and Technology*, vol. 9, no. 3, pp. 175–184, 1996.

[27] G. Peterson and J. Ha, "Capillary performance of evaporating flow in micro grooves: an approximate analytical approach and experimental investigation," *Journal of Heat Transfer*, 1998.

[28] M. M. Weislogel, "Capillary flow in interior corners: The infinite column," *Physics of Fluids*, vol. 13, no. 11, pp. 3101–3107, 2001.

[29] M. M. Weislogel, "Capillary flow in containers of polygonal section," *AIAA journal*, vol. 39, no. 12, pp. 2320–2326, 2001.

[30] M. M. Weislogel, "Some analytical tools for fluids management in space: Isothermal capillary flows along interior corners," *Advances in Space Research*, vol. 32, no. 2, pp. 163–170, 2003. Gravitational Effects in Physico-Chemical Processes.

[31] J. Li, X. Chen, and Y. Huang, "The review of the interior corner flow research in microgravity," *Procedia Engineering*, vol. 31, pp. 331–336, 2012.

[32] M. M. Weislogel, E. Thomas, and J. Graf, "A novel device addressing design challenges for passive fluid phase separations aboard spacecraft," *Microgravity Science and Technology*, vol. 21, no. 3, p. 257, 2009.

[33] J. Li, X. Chen, Y. Huang, and Y. Bai, "Study on asymmetric interior corner flow in microgravity condition," *Science China Technological Sciences*, vol. 55, no. 8, pp. 2332–2337, 2012.

[34] Y. Wei, X. Chen, and Y. Huang, "Interior corner flow theory and its application to the satellite propellant management device design," *Science China Technological Sciences*, vol. 54, no. 7, pp. 1849–1854, 2011.

[35] Y. Chen, N. Tavan, and M. M. Weislogel, "A mean curvature model for capillary flows in asymmetric containers and conduits," *Physics of Fluids*, vol. 24, no. 8, p. 082111, 2012.

[36] Y. Chen, M. M. Weislogel, and D. Bolleddula, "Capillary flow in cylindrical containers with rounded interior corners," in *45th AIAA Aerospace Sciences Meeting and Exhibit*, p. 745, 2007.

[37] Y. Chen, M. M. Weislogel, and C. L. Nardin, "Capillary-driven flows along rounded interior corners," *Journal of Fluid Mechanics*, 2006.

[38] Y. Tang, X. Chen, and Y. Huang, "Capillary flow rate limitation in asymmetry open channel," *Chinese Journal of Acheneronautics*, vol. 28, no. 3, 2015.

[39] S.-K. Su and C.-L. Lai, "Interfacial shear-stress effects on transient capillary wedge flow," *Physics of Fluids*, vol. 16, no. 6, pp. 2033–2043, 2004.

[40] E. L. Golliher, C. Nardin, and M. M. Weislogel, "Capillary driven flows along differentially wetted interior corners," Technical Memorandum CR213799, Nasa, Glenn Research Center Cleveland, OH, United States, 2005.

[41] J. Zhou and M. Doi, "Universality of capillary rising in corners," *Journal of Fluid Mechanics*, vol. 900, p. A29, 2020.

[42] N. C. White and S. M. Troian, "Why capillary flows in slender triangular grooves are so stable against disturbances," *Physical Review Fluids*, vol. 4, no. 5, p. 054003, 2019.

[43] F. Mayer, J. McGrath, and J. Steele, "A class of similarity solutions for the nonlinear thermal conduction problem," *Journal of Physics A: Mathematical and General*, vol. 16, no. 14, p. 3393, 1983.

[44] K. Zischka and P. Chow, "On nonlinear initial boundary value problems of heat conduction and diffusion," *SIAM Review*, vol. 16, no. 1, pp. 17–35, 1974.

[45] R. C. McOwen, *Partial differential equations: methods and applications*. Prentice-Hall, 2004.

[46] L. C. Evans, "Partial differential equations," *Graduate studies in mathematics*, vol. 19, no. 2, 1998.

[47] H. Brezis, *Functional analysis, Sobolev spaces and partial differential equations*. Springer Science & Business Media, 2010.